IDENTIFICATION OF FORCE COEFFICIENTS FROM A GAS ANNULAR SEAL-EFFECT OF TRANSITION FLOW REGIME TO TURBULENCE

David Ransom
Dr. Luis San Andrés

April 1997

TRC-SEAL-4-97

Texas A&M University
Mechanical Engineering Department

IDENTIFICATION OF FORCE COEFFICIENTS FROM A GAS ANNULAR SEAL - EFFECT OF TRANSITION FLOW REGIME TO TURBULENCE

by

David L. Ransom
Research Assistant
and
Luis San Andrés
Associate Professor, P.I.
Plank Co. Faculty Fellow

A Research Progress Report to the
Turbomachinery Research Consortium

TRC-Seal-4-97

Subject: Seals

May 1997

TABLE OF CONTENTS

NOMENCLATURE

a	=	sound speed of air [L/T]
C_{ij}	=	seal damping coefficients [M/T], $i,j = X,Y$
C_{hi}	=	support damping coefficient [M/T], $i = X,Y$
c	=	seal radial clearance [L]
D	=	seal journal diameter [L]
F_j	=	external impact force [ML/T^2], $j = X,Y$
FFT	=	fast fourier transform
H_{ij}	=	frequency domain impedance coefficients [M/T^2], $i,j = X,Y$
j	=	$\sqrt{-1}$
K_{ij}	=	seal stiffness coefficients [M/T^2], $i,j = X,Y$
L	=	seal length [L]
M_e	=	V_e/a. Mach number at seal exit
M_{ij}	=	seal inertia coefficients [M], $i,j = X,Y$
M_h	=	seal housing mass [M]
$\dot{m}$	=	mass flow rate through seal [M/T]
P_{atm}	=	atmospheric (seal exit) pressure [M/LT^2]
P_{supply}	=	supply pressure to seal inlet [M/LT^2]
P_{ratio}	=	P_{supply}/P_{atm}, pressure ratio
P_1	=	seal inlet pressure [M/LT^2]
P_2	=	air line pressure before flow meters [M/LT^2]
P_3	=	air line pressure after flow meters [M/LT^2]
Re_{axial}	=	$\dot{m}/\pi D\mu = \rho V_e c/\mu$ Axial flow Reynolds number.
U_f	=	uncertainty of measurements. Subscript indicates measurement type.
V_e	=	bulk-flow velocity at seal exit [L/T]
X,Y	=	seal displacements about equilibrium position [L].
$\dot{X},\dot{Y}$	=	seal velocities in the X,Y directions [L/T]
$\ddot{X},\ddot{Y}$	=	seal and housing accelerations in the X,Y directions [L/T^2]
T_1	=	inlet temperature of air [F]
T_2	=	lubricant temperature at exit of roller bearing [F]
δ_{ij}	=	Dirac Delta function
ρ	=	air density [M/L^3]
μ	=	viscosity of air [M/LT]
σ	=	standard deviation
ω	=	frequency [1/T]

Subscripts

atm	=	refers to atmospheric pressure
axial	=	refers to axial flow direction
d	=	refers to displacement measurement
h	=	refers to housing support parameters
i,j	=	corresponds to X,Y combinations. First subscript indicates direction of motion. Second subscript indicates direction of force.
ratio	=	refers to ratio of supply and atmospheric pressures
supply	=	refers to supply pressure at inlet of seal

LIST OF FIGURES

LIST OF TABLES

EXECUTIVE SUMMARY

Experiments to identify stiffness and damping force coefficients of a smooth surface, gas (air) annular seal of uniform clearance are presented. Calibrated impact guns excite a housing holding the test seal, and the seal displacement and acceleration time responses in two orthogonal directions are measured. A frequency domain parameter identification procedure allows the determination of the seal dynamic force coefficients over a frequency range. The current tests are carried out in preparation for further experiments with gas labyrinth seals and *TAMseals*.

The experiments include tests without journal rotation and with rotation at 3,600 rpm, and centered and off-centered seal positions to 50% of the radial clearance. The pressure drop across the seal is controlled by increments in the inlet supply pressure to values three times the exit (ambient) pressure. Test flow rates and direct damping coefficients increase as the supply pressure raises. The identified seal stiffness coefficients show a peculiar behavior with a dramatic reduction to null and negative values at a pressure ratio equal to 2.0. Predictions from a computer model accounting for flow in the transition regime to full turbulence show a favorable agreement with the identified force coefficients. Measurements for seal off-centered conditions could not be performed for pressure ratios above 2.5 since a sonic flow conditions is suspect to create self-excited seal motions.

The report includes a review of test and identification procedures for fluid film bearing dynamic force coefficients, a description of the test rig and the parameter identification method, and a discussion on the uncertainty of the measurements. Test values for the seal mass flow rate and estimated force coefficients are accompanied by computational predictions and a thorough discussion. Excellent coherence of the test responses to the applied loads and goodness of fit for a linear analytical model representing the test system validate the identified force coefficients. The measurements also validate predictions from a computational bulk-flow model accounting for a laminar to turbulence transition flow regime.

INTRODUCTION

Hydrodynamic bearings and seals have a profound effect on the rotordynamic performance of a rotor-bearing system. Fluid film bearing reaction forces are general functions of the fluid properties, operating conditions and geometric configuration. For small amplitudes of journal motion about an equilibrium position these bearing forces are generally represented as linearized bearing stiffness, damping and inertia force coefficients (Lund, 1987, Childs, 1993).

$$\begin{bmatrix} F_x \\ F_y \end{bmatrix} = \begin{bmatrix} K_{xx} & K_{xy} \\ K_{yx} & K_{yy} \end{bmatrix} \begin{bmatrix} X \\ Y \end{bmatrix} + \begin{bmatrix} C_{xx} & C_{xy} \\ C_{yx} & C_{yy} \end{bmatrix} \begin{bmatrix} \dot{X} \\ \dot{Y} \end{bmatrix} + \begin{bmatrix} M_{xx} & M_{xy} \\ M_{yx} & M_{yy} \end{bmatrix} \begin{bmatrix} \ddot{X} \\ \ddot{Y} \end{bmatrix} \qquad (1)$$

These bearing parameters, typically regarded as frequency independent, are necessary to predict critical speeds and logarithmic decrements of rotors supported on fluid film bearings. The direct coefficients characterize a force that is in the same direction as the journal motion; whereas the off diagonal (cross-coupled) coefficients represent forces that although proportional to the generalized displacement, velocity or acceleration, act in a direction perpendicular to it. The linear model in the above equation is valid only for rigid surface seals operating at sufficiently low frequencies and with incompressible fluids.
An experimental procedure to identify the force coefficients must be proven reliable, repeatable, and certain.

A parameter identification procedure comprises of the method to excite the bearing or seal and the method to extract the bearing or seal parameters from the response measurements. Software and hardware limitations aside, the methods and procedures selected have the largest effect on the quality of the results. Here, three methods of forced excitation and two methods of parameter identification are examined. Each excitation method can be combined with either identification procedure. However, these are not com-

pletely independent of each other. For instance, tests with impact load excitations excite transient journal motions which can be stored as time domain records or frequency domain spectra, depending on the identification procedure selected. Thus, even though the forced excitation methods and the parameter identification methods are discussed separately, it is important to remember that they are closely related.

A review of past literature shows that three techniques of bearing excitation prevail. These correspond to vibratory loads (shakers), unbalance loads and impact loads. The number of papers available on vibratory loading indicates this to be the dominate method to date. However, this method requires sophisticated test set ups. For example, the stinger (which attaches the shaker to the test subject) must be rigid in the direction of loading, but fully flexible in all orthogonal directions. Mitchell and Elliott (1984) provide design guidelines for stinger flexural stiffness and exciter support stiffness.

Morton (1971) reports measurements made on an industrial size journal bearing using a single shaker to excite the bearing. A static load is applied using nitrogen pressurized bellows (50 tons maximum). The dynamic load is provided by an electrohydraulic shaker with a maximum load of 2 tons and top frequency of 50 Hz. Measured parameters include static force, dynamic forces, and bearing position relative to the journal. With only one shaker, it is not feasible to provide movement in only one direction without physically constraining the system. Therefore, response motions in two orthogonal directions are measured for excitation frequencies different than the rotational speed. The amplitude of the dynamic force (2 tons) provides a linear response and also a good signal to noise ratio. The resulting stiffness and damping values are found to be significantly lower than theoretical values. Morton believes theory to be deficient and states that the experimental results compare well with unbalance tests performed on a similar bearing.

Parkins (1979) introduces the selected orbit technique, a variation of the shaker method, which requires a straight line journal orbit in either one of two orthogonal directions. The magnitude and phase of each shaker are controlled so that the combined forces provide a straight line motion of the test bearing. The time response show specific times when the journal displacement (relative to a static equilibrium) is null, and other times when the velocity is zero. Thus, measurements in two planes (*X and Y*) render eight separate equations from which eight dynamic force coefficients (stiffness and damping) are extracted. These linearized force coefficients are regarded as constants about a static equilibrium position. Parkins measurements demonstrate that the linear assumption is not valid for motions about journal eccentricity ratios greater than 0.78, and thus, first order corrections to the test stiffness and damping coefficients are then needed. Parkins also shows static force coefficients extracted from an incremental load method on the same test apparatus. The load is applied by adding weights to a cable-pulley system. Four stiffness coefficients are determined with one added weight in each direction and measured displacements in both directions. The dynamic values of stiffness correlate well with the incremental loading values wherever a direct comparison is made. The cross-coupled stiffness and damping coefficients (K_{XY} and C_{XY}) are shown to be nonlinear at eccentricity ratios greater than 0.78. All stiffness and damping coefficients are nonlinear for journal eccentricity ratios greater than 0.86 and 0.90 respectively. Unfortunately, no uncertainty analysis is provided for the test data.

Brockwell, Kleinbub and Dmochowski (1990) report on measurements of the stiffness and damping coefficients for a five shoe tilting pad bearing using the selected orbit technique. Two shakers excite the bearing at a frequency synchronous with shaft speed. The maximum available static load is 18,000 N and maximum available dynamic load is 1,700 N. Preliminary measurements show that the there are no cross-coupling forces generated by the test bearing, and therefore no cross-coupled terms are identified. Although no uncertainty analysis is presented, the data appears to be repeatable and correlates well with the full film (2π) bearing theory which includes thermal expansion of the pads, shaft and housing.

Parkins (1995) reports on a novel form of the selected orbit technique as a figure eight (not a straight line). The figure eight pattern only requires one orbit containing non-parallel, but not necessarily orthogonal, overlapping straight lines for part of its length. From this orbit, four damping coefficients are determined in a skewed coordinate system. Parkins establishes a routine to translate these coefficients to

the more useful coefficients in the horizontal and vertical directions. An uncertainty analysis claims error in the setting of the orbit shape and the axes conversion, and amounting to no more than 10% for three of the four estimated damping coefficients. In the tests, the experimental orbit data is not the most desirable accounting for a large percentage of the error. Parkins suggests that better figure eight's can be achieved to render more precise measurements.

Childs, Nelson, Nicks, Scharrer, Elrod and Hale (1986) describe a test apparatus to extract rotordynamic coefficients from annular gas seals using a shaker in the horizontal direction. Eccentric operation is achieved by a cam displacing the shaft in the vertical direction. By exciting the system at one frequency, both stiffness and damping coefficients are identified. The extracted coefficients are assumed to be linear within a prescribed frequency range. Nelson, Childs, Nicks and Elrod (1986) measure leakage and the rotordynamic force coefficients of a plain annular seal and a convergent geometry seal using the test rig described in the above report. Tests are performed at various pressure ratios, shaking frequencies, and inlet pre-swirl conditions. The stiffness and damping coefficients are displayed as a function of pressure ratio. For each condition of fluid pre-swirl, the stiffness coefficients show clear trends. The damping coefficients do not vary with varying inlet pre-swirl condition. The measurement uncertainty is given by error bars on each stiffness and damping coefficient. The authors show that damping measurements have a higher uncertainty than stiffness measurements.

A second method of dynamic force excitation is due to a rotating imbalance mass. Using imbalance forcing is much less sophisticated than the shaker approach, but can require large amounts of testing time if numerous masses are used or if results for various rotational frequencies are desired (Goodwin, 1991). Hagg and Sankey (1956) report on tests for a 150° hydrodynamic journal bearing and a four pad pivot bearing using this method. The rotor is mounted vertically and a static load (simulating rotor weight) is applied with a mass lever system. Vibrations are measured using the wattmeter technique, so only fundamental vibrations synchronous with journal speed are observed. The data is presented in dimensionless form for easiness of comparison with other works. The results for the test journal bearing show considerable scatter, and the authors estimate uncertainties of 10 to 20%. The results for the pivot pad bearing show much less scatter and also follow theory quite well. The uncertainties are mainly due to measurement errors.

Stanway (1983) reports on a variation of the unbalance mass testing method which allows for testing of rotating machinery already in operation. Time domain numerical responses to imbalance in a rotor supported on a squeeze film damper are generated. The analysis requires of initial conditions for amplitude of vibration and journal velocity (in two orthogonal directions), system natural frequency, running speed, and values for all four damping coefficients. The computations render time domain displacements in two orthogonal directions. Stanway adds noise to the responses for a more precise simulation of actual conditions. In the identification procedure, an initial state vector includes initial guesses for displacement, velocity, and the four damping coefficients. Initial damping values twice the actual values are used to demonstrate the robustness of the procedure. The results show that after 100 ms, the methods is able to identify all four coefficients within 10 %. However, the procedure does not render stiffness coefficients, and the author recommends determining these parameters from an incremental loading test.

Tieu and Qiu (1994) use the unbalance mass method to extract sixteen rotordynamic coefficients from two hydrodynamic journal bearings. Two unbalance masses are used simultaneously. The entire procedure requires five tests, the first with no added masses (baseline response). The second test is carries out with two masses at right angles. For the third test, the same two masses in the second test merely switch positions with each other. The fourth test corresponds to two masses directly opposing each other. Finally, in the fifth test, the same two masses from the fourth test switch places with each other. For each test, orthogonal displacements and one pulse per revolution are recorded. This information is transformed to the frequency domain for the analysis procedure. All sixteen coefficients are successfully identified and compared to theoretical values. As also determined in other relevant works, the stiffnesses better match the theoretical values than the damping coefficients, particularly in the region of journal eccentricities below

50% of the bearing clearance. The authors state that the response produced by placing the masses at right angles to each other is greater than when they are out of phase by 180°. If a limited number of tests is available, then just the two tests with the masses at right angles (and the baseline test) are enough to obtain reasonable results. No values are presented on the uncertainty of the coefficients for either method.

The third method of excitation is the impact or impulse method. The impact load has the distinct advantage of exciting a wide range of frequencies at one time. This range is dictated by the softness of the impact tip and the velocity of the impact. Nordmann and Schollhorn (1980) report on impact testing of a rotor supported by two fluid film bearings. The measured parameters are impact force and rotor displacements. The impact is measured by an accelerometer attached to the hammer. Displacement is measured at either end of the shaft by eddy current displacement sensors. The time data is transformed to the frequency domain and recorded on tape. Averaging several impacts eliminates the "noise" from the response data. For comparison, a linear model is used to numerically produce a frequency response to an impulse. The values for stiffness and damping of the model are altered so that the transfer function of the linear model matches the transfer function of the rotor-bearing system. Stiffness values show very little scatter, however damping values show large amounts of scatter.

Qiu and Tieu (1993) report on further measurements made using the impact method. The authors claim that their particular experiment is more applicable to industry because a rotor-bearing system with two asymmetric support bearings could be tested. By acquiring three sets of data, all sixteen rotordynamic coefficients for the rotor-bearing system can be identified. The first set of data is the initial vibration displacements (due to unbalance vector, u). The second set is the response to an impact in the X direction, and the third is the response to an impact in the Y direction. After transforming all data to the frequency domain, the baseline vibration frequency response is subtracted from the impact frequency responses. This decreases the noise effect of the synchronous vibration response. Next, all sixteen terms are extracted using the method described. The extracted parameters (force coefficients) are used to calculate time and frequency responses using a linear model. Then these are compared to the actual acquired time and frequency responses. The authors report that the model results do compare well with the acquired data and correlate well with theory.

As stated earlier, the method of forced excitation is only one part of the parameter identification process. The actual identification of the rotordynamic force coefficients requires of a procedure to analyze the test data in either the time domain or the frequency domain. Hagg and Sankey (1956) record time responses of journal motion for a bearing subjected to both static and imbalance loads. By defining a cartesian coordinate system with the (X,Y) axes along the major and minor axes of the journal orbit, the authors are able to determine the exact instants in time when the journal displacements are zero on each axis. The damping and stiffness coefficients are determined from the solution of two uncoupled steady state equations of journal motion. The authors state that the inaccuracies in the parameter values are mostly due to phase measurement errors.

Parkins (1979,1981,1995) uses the selected orbit technique which allows for exact measurement of times when journal velocities and displacements are null. However, Parkins uses two coupled equations to describe the journal motion, thus resulting in direct and cross-coupled terms. As mentioned previously, Parkins measures non-linear coefficients, so all values are presented in terms of a zero value and a gradient. The test zero values show very little spread, while the gradient terms show large scatter and do not seem useful. Parkins concludes that the measurements could have been improved with an on-line subtraction of journal center coordinates (runout removal).

Brockwell, Kleinbub and Dmochowski (1990) come to similar conclusions after testing a tilting-pad bearing. The model uses two uncoupled equations of motion because the tests show no cross-coupled force coefficients. Otherwise, the technique is the same as Parkins'. The results show some scatter but certainly at acceptable levels. The synchronous signal from the displacement sensors makes it difficult to identify the point in time when the bearing center passes through the steady state position. The authors

conclude that the shaft runout noise combined with the noise from the support bearings explain the errors in stiffness and damping measurements.

In an effort to overcome the synchronous noise problem described above, Burrows and Sahinkaya (1982) perform an analysis of a frequency-domain estimation method. The system is modeled by two coupled equations of motion excited by a Schroeder-phased harmonic signal which contains 100 harmonics. The identification procedure requires four inputs, two displacement time records, and two force time records (one for each orthogonal direction). The input signals are then transformed to the frequency domain and used to fill two matrices, one containing displacements and applied forces, and another containing displacements only. These two matrices can be applied to a least squares estimator equation which renders the eight rotordynamic force coefficients. In an effort to estimate the effect of bias on parameter estimation, another form of the least squares estimator is used which includes a noise term. In one set of response data, a noise level of 5% completely destroys the method's ability to estimate parameters. However, by taking an average frequency response, the authors found that the effect of 5% noise is almost removed. For another test, the authors use actual experimental data to determine the coefficients of a squeeze-film damper bearing. The results of this frequency technique are compared with the results of a time domain method used on the same data. The frequency domain method shows much less scatter than the time domain method. In addition, three of the four damping coefficients obtained with the frequency domain method are found to be in close agreement with the π-film theory for squeeze-film damper bearings.

Tieu and Qiu (1994) measure a rotor-bearing system forced response to imbalance and transform it to the frequency domain where bearing impedances are identified. To prove the ability of the *FFT* procedure, the authors plot the inverse *FFT* of each measured signal against the original time data and show there is virtually no difference. The test results appear to be repeatable, although no particular information is given regarding the uncertainty of the estimated force coefficients. In addition, the frequency domain least squares estimation requires much less effort than does a non-linear curve fit of time domain data.

Rouvas (1993) uses the power spectral density method to identify the rotordynamic force coefficients of hydrostatic bearings. Rouvas states that although the method is intended for random vibrations, it can be used successfully for deterministic vibrations as well. There are two distinct advantages to the power spectral density method. First of all, if two signals are statistically independent, then the cross spectral density of those two signals is zero. This characteristic allows the effect of noise to be eliminated from the frequency response function. Time domain analysis methods require that for multiple excitations each excitation must start at a similar point in the cycle and the excitations must have the same magnitude. The power spectral density method does not require either of the two previous conditions.

Ewins (1986) discusses coherence as an important measure of causality between an output response and an input force. If the output response is due solely to the input force, then the coherence has a value of unity. If the output response is not related to the input force the coherence is less than one. Coherence does vary with frequency. There are several possible reasons to have poor coherence (<1), many are related to failure of the instrumentation, but the most relevants are related to measurements contaminated with extraneous *noise* during the testing. Therefore, signal coherence is a good tool for verifying the quality of the measurement although it does not provide information regarding the cause of poor measurements.

TEST RIG DESCRIPTION

A cutaway view of the test rig is shown in Figure 1. A 7.5 kWatt (10 hp) DC motor drives the shaft via a belt-pulley system. The maximum speed of the test shaft is 14,400 rpm. The base block is made of steel and weighs 104 kg (230 lb). The test shaft is held in the base by three precision angular contact ball bearings. Lubrication for the ball bearings is provided by a dedicated oil pump with a 144 liter (38 gallon) reservoir. A journal is mounted on the end of the shaft with a key and a retaining nut. The natural fre-

quency of the test shaft with the journal in place is 417 Hz. The measured mechanical runout of the shaft at the top is 25.4 μm (0.001 inches).

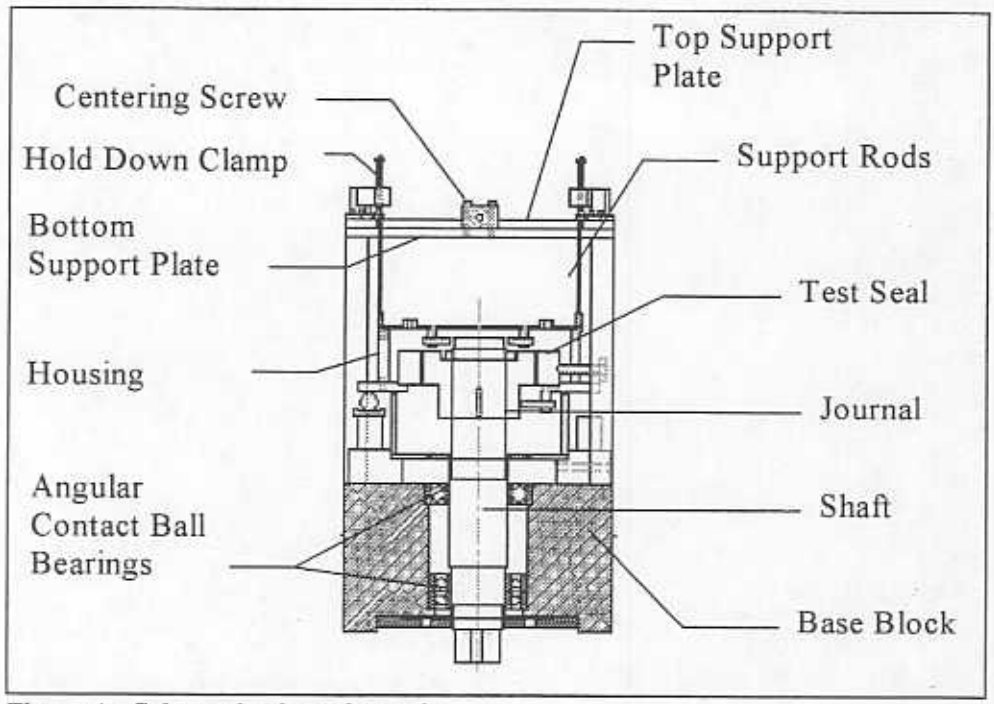

Figure 1 - Schematic view of test rig

The aluminum housing containing the test seal is suspended by four threaded mild steel rods, 8 mm (5/16 inches) in diameter and 152.4 mm (6.0 inches) long. These rods are bolted to the top support plate which rests flat on the bottom support plate. Figure 2 shows a view of the top and bottom plates and the four position screws allowing the relative motion of the top plate and centering of the seal relative to the journal. The mating surfaces for both plates (each 0.0127 m (0.5 inches) thick) are flat within 25.4 μm (1 mil) so as to insure minimal friction when sliding. The four clamps hold the top plate in its desired place, and prevent its raise when the housing is pressurized.

The test seal element is a smooth surface plain annular seal with a uniform clearance and dimensions as listed in Table 1. The aluminum housing holds the seal. Four eddy current displacement sensors and a strain gage pressure transducer are fastened to the housing cap. Two 23 gr piezoelectric accelerometers are mounted to the side of the housing with magnetic bases. Figure 3 shows the position of the displacement sensors and accelerometers.

Table 1 - Test seal dimensions

Outer Diameter	17.780 cm (7.000 in)
Inner Diameter	12.725 cm (5.010 in)
Journal Diameter (D)	12.687 cm (4.995 in)
Radial clearance (c)	190 μm (7.5 mils)
Length (L)	4.064 cm (1.6 in)
material	Brass

uncertainty ±12.7 μm (0.5 mils)

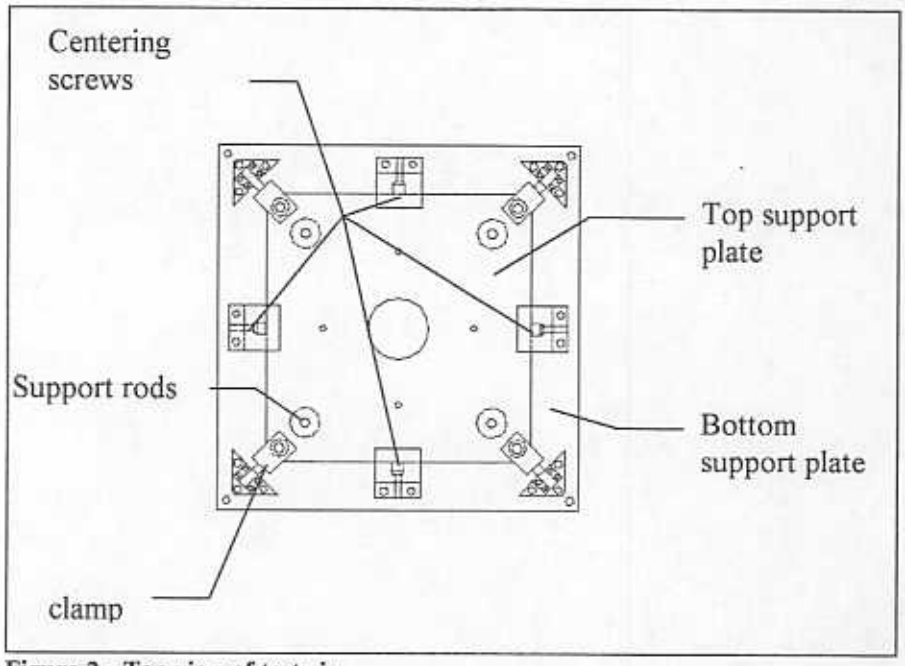

Figure 2 - Top view of test rig

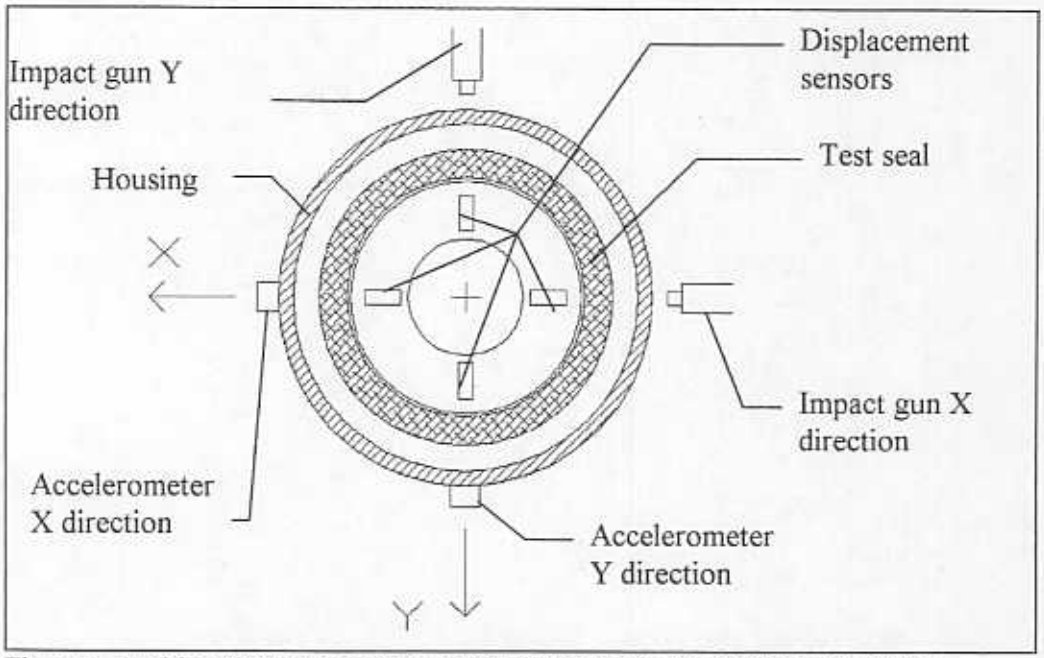

Figure 3 - Position of displacement and acceleration sensors and coordinate system

The housing mass equals 10.0 kg and includes all transducers attached to the housing, the seal ring element, and a fraction (33/140) of the rods masses. The housing and rods structural stiffness and damping are measured with several techniques. First, the stiffness is measured by applying static forces to the housing along the *X* and *Y* directions, and measuring the displacement (in the same load direction) with the eddy current sensors installed in the housing (see Figure 3). The structural damping coefficient is first measured by impacting the housing and recording the time domain displacement response with a data acquisition plotter. The logarithmic decrement is extracted from the peak response ratios in the time response. Secondly, the structure damping is estimated from the frequency domain (displacement/load) transfer function due to 8 repeated impacts imparted with an instrumented hammer. Finally, a Zonic

PC7000 Multi-Channel *FFT* Analyzer is used to measure the stiffness and damping coefficients simultaneously. A description of the data acquisition system is given later. Table 2 lists the identified structure stiffness $(K_{ih})_{i=X,Y}$ and damping $(C_{ih})_{i=X,Y}$ values, and includes the uncertainty for each measurement. The housing and rod structure has a fundamental natural frequency of just 30 Hz since the support rods stiffnesses are not large. The damping coefficient from the housing assembly is small (about 4% of critical damping), and typical of steel structures. The results from Table 2 indicate that the multi-channel data acquisition system combined with the parameter identification technique described below provides the most certain damping coefficients estimates.

Table 2 - Stiffness and damping from seal housing structure.

Method	Parameter	Value	Uncertainty
Static Displacement	K_{hX}	264 kN/m (1510 lb/in)	5.7 %
	K_{hY}	249 kN/m (1424 lb/in)	5.7 %
Multi-Channel *FFT*	K_{hX}	278 kN/m (1590 lb/in)	2.2 %
	K_{hY}	252 kN/m (1440 lb/in)	2.2 %
Log. Dec.	C_{hX}	124 N sec/m (0.71 lb sec/in)	11.7 %
	C_{hY}	105 N sec/m (0.60 lb sec/in)	13.5 %
Transfer Function	C_{hX}	131 N sec/m (0.75 lb sec/in)	13.3 %
	C_{hY}	103 N sec/m (0.60 lb sec/in)	12.4 %
Multi-Channel *FFT*	C_{hX}	159 N sec/m (0.91 lb sec/in)	5.0 %
	C_{hY}	113 N sec/m (0.65 lb sec/in)	5.0 %
Digital Scale	Mass	10.0 kg (22.0 lb)	1%

The highlighted values are subtracted later from the estimates of total seal + structure force coefficients in order to isolate the seal force coefficients

The discharge lubricant temperature from the rolling element bearings in the test rig base is measured with a K-type thermocouple. Pressurized air is delivered to the seal through a flexible hose. The air supply line contains a type-K thermocouple for measurement of temperature, and a Headland visual flow meter and a turbine type flow meter. A pressure regulator well upstream of the test seal allows regulation of the air pressure. The inlet air pressure to the seal is measured with a strain gauge pressure transducer mounted on the housing cap. The air flow through the seal exhausts to atmospheric conditions.

The data acquisition is performed by an 8 channel simultaneous sampling *FFT* analyzer with a maximum rate of 20,000 samples/sec. Table 3 lists the acquisition parameters used in the testing. The sampling rate is a compromise between resolution for the measurement (in time) of the impact loads and resolution of the seal displacements and accelerations frequency spectra. Impacts imparted with soft tips in the guns last ~3 milliseconds, while the seal dynamic motion lasts well over 1.0 sec. A sampling rate of 6,600 samples/sec leads to a resolution in the frequency domain of 0.81 Hz, and with the impact described by 20 discrete data points.

Table 3 - Data acquisition parameters

Acquisition Parameter	Value
Sampling frequency	6,600 samples/sec
Number of samples	8,192 per test
Total sampling time	1.24 sec
Full scale voltage	4.7 volts all channels
Windowing	none
Pre-trigger	5 samples

The full scale voltage (FSV) is an important parameter and must be considered carefully. In terms of measurement accuracy it is best for each motion transducer to use as much of the FSV as possible. Different transducers operate in different ranges and the data acquisition system allows each channel to have a different range. In these tests, all D/A channels must have the same FSV to fit the requirements of the

procedure implemented for post processing operations. The piezoelectric accelerometers produce significantly smaller voltage signals than the eddy current sensors and the impact gun load cells. Therefore, the accelerometer outputs are pre-amplified by a factor of 10 with a signal conditioner. The sensitivity for each transducer is listed in Table 4.

Table 4 - Transducer gains

Transducer	Gain
Displacement X	124 μm/volt
Displacement Y	126 μm/volt
Acceleration X	9.225 g/volt
Accceleration Y	9.461 g/volt
Force X	44.11 N/volt
Force Y	43.67 N/volt

The data acquisition is initiated by an increase of 7% of FSV on the impact load cell channel. However, since the impacts last very shortly, the data points before the trigger 7% value are also required. A built-in pre-trigger function allows to recover the date to the instant when the impact just initiates. Experiments show that a 7% of FSV for the impact loads amounts to the first 5 data points. Therefore, the pre-trigger is set to exactly 5 data points.

TEST PROCEDURE

The experiments are performed without journal rotation (0 rpm) and at a journal speed of 3,600 rpm. The static position of the seal with respect to the journal is either centered or off-center in the X direction by one half (50%) of the clearance. The off-center operation is achieved through adjustment of the centering screws on the top support plate (see Figure 2). A *pressure ratio* is defined as the ratio of the absolute supply pressure (P_{supply}) to the absolute discharge pressure (P_{atm}) which corresponds to ambient conditions. All experiments are conducted at a mean air temperature equal to 73 °F (23 °C). Table 5 lists the conditions for all tests conducted. Those tests with an asterisk in the *pressure ratio* column are performed twice, and therefore show two data points in the results.

The gun triggering and the data acquisition are fully controlled from the computer. For each impact in either the X or Y directions, the signals from the gun load cell, two accelerometers, and two displacement sensors are acquired and stored temporarily. The seal dynamic responses are evaluated graphically before permanent storage. The impact test is repeated if the response is not acceptable. Impact responses are discarded for various reasons like double impact, impact too large, impact too small, or a failed transducer during acquisition. The entire frequency domain response data is saved upon acceptance. Every test consists of 32 impacts in each direction (X or Y) for a given test condition (journal speed, seal static position, and pressure ratio).

Table 5 - Test conditions

Journal speed (RPM)	Seal static position	Pressure ratio (P_{supply}/P_{atm})
0	Centered	1.25
		1.5*
		1.75
		2.0*
		2.25
		2.5*
		3.0*
0	Off-Center 50% of radial clearance	1.5
		2
		3.0
3,600	Centered	1.5*
		2.0*
		2.5*
		3.0*

PARAMETER IDENTIFICATION METHOD

The identification of the seal dynamic force coefficients is performed by analysis of the seal forced response and impact load in the frequency domain. The housing and seal ring, considered as a rigid mass supported by the rods' structure and the annular seal, move in a horizontal plane under the forced excitation of the impact guns. The equations of motion for small amplitudes about an equilibrium position are described in linear form by,

$$\begin{aligned}\left(M_{XX}+M_h\right)\ddot{x}+M_{XY}\ddot{y}+\left(C_{XX}+C_{hX}\right)\dot{x}+C_{XY}\dot{y}+\left(K_{XX}+K_{hX}\right)x+K_{XY}y=f_X\\ \left(M_{YY}+M_h\right)\ddot{y}+M_{YX}\ddot{x}+\left(C_{YY}+C_{hY}\right)\dot{y}+C_{YX}\dot{x}+\left(K_{YY}+K_{hY}\right)y+K_{YX}x=f_Y\end{aligned} \tag{2}$$

where $\{fi\}_{I=X,Y}$ are external forces, M_h is the combined housing and seal mass, $\{K_{hi}, C_{hi}\}_{I=X,Y}$ are the support structure stiffness and damping coefficients (see Table 2), and $\{K_{ij}, C_{ij}, M_{ij}\}_{i,j=X,Y}$ are the annular seal stiffness, damping and inertia force coefficients, respectively. The model for equations (2) assumes the seal journal motion in the lateral directions (X,Y) to be negligible and does not include the effects of spurious (random) noise due to fluctuations in the air pressure and local flow turbulence. The journal lateral motion is indeed small since the shaft support is nearly rigid at the test conditions. However, some amplitude of shaft runout (25.4 μm (1.0 mil)) at synchronous frequency is present in the tests at 3,600 rpm. The effects of random noise are minimized by the averaging procedure of the 32 impact responses and seal forced frequency responses. Equations (2) in matrix form become

$$\begin{bmatrix}M_{XX}+M_h & M_{XY}\\ M_{YX} & M_{YY}+M_h\end{bmatrix}\begin{bmatrix}\ddot{x}\\ \ddot{y}\end{bmatrix}+\begin{bmatrix}C_{XX}+C_{hX} & C_{XY}\\ C_{YX} & C_{YY}+C_{hY}\end{bmatrix}\begin{bmatrix}\dot{x}\\ \dot{y}\end{bmatrix}+\begin{bmatrix}K_{XX}+K_{hX} & K_{XY}\\ K_{YX} & K_{YY}+K_{hY}\end{bmatrix}\begin{bmatrix}x\\ y\end{bmatrix}=\begin{bmatrix}f_X\\ f_Y\end{bmatrix} \tag{3}$$

Let

$$X(\omega)=FFT(x(t)),\quad Y(\omega)=FFT(y(t)),\quad F_i(\omega)=FFT(f_i(t)) \tag{4}$$

be the *Fourier transforms* of the dynamic seal responses and of the applied impact loads, respectively. By definition,

$$\dot{X} = j\omega X \qquad \dot{Y} = j\omega Y$$
$$\ddot{X} = -\omega^2 X \qquad \ddot{Y} = -\omega^2 Y \tag{5}$$

where $j = \sqrt{-1}$ and (ω) is the frequency. Application of the *Fourier transform* to the linear ordinary differential equations (3) gives the following set of algebraic equations in the frequency domain,

$$-\omega^2\begin{bmatrix} M_{XX}+M_h & M_{XY} \\ M_{YX} & M_{YY}+M_h \end{bmatrix}\begin{bmatrix} X \\ Y \end{bmatrix} + j\omega\begin{bmatrix} C_{XX}+C_{hX} & C_{XY} \\ C_{YX} & C_{YY}+C_{hY} \end{bmatrix}\begin{bmatrix} X \\ Y \end{bmatrix} + \begin{bmatrix} K_{XX}+K_{hX} & K_{XY} \\ K_{YX} & K_{YY}+K_{hY} \end{bmatrix}\begin{bmatrix} X \\ Y \end{bmatrix} = \begin{bmatrix} F_X \\ F_Y \end{bmatrix} \tag{6}$$

Complex *impedances* $\{H_{ij}\}_{i,j=X,Y}$ are defined as

$$H_{ij} = \left[\left(K_{ij} + K_{hi}\delta_{ij}\right) - \omega^2\left(M_{ij} + M_h\delta_{ij}\right)\right] + j\omega\left(C_{ij} + C_{hi}\delta_{ij}\right) \tag{7}$$

where $\delta_{ij} = 1$ for $i=j=X,Y$; 0 otherwise. The impedances are composed of real and imaginary parts, both functions of frequency (ω). The real part denotes the dynamic stiffness, while the imaginary part is proportional to the damping coefficient. Substitution of the impedance definitions into the frequency domain equations (6) leads to:

$$\begin{bmatrix} H_{XX} & H_{XY} \\ H_{YX} & H_{YY} \end{bmatrix}\begin{bmatrix} X \\ Y \end{bmatrix} = \begin{bmatrix} F_X \\ F_Y \end{bmatrix} \tag{8}$$

These represent two algebraic equations and four unknown impedances $(H_{ij})_{i,j=X,Y}$. For two independent impact excitations $(f_X,0)^T$ and $(0,f_Y)^T$, the equations of motion are:

$$\begin{bmatrix} X_X & Y_X \\ X_Y & Y_Y \end{bmatrix}\begin{bmatrix} H_{XX} \\ H_{XY} \end{bmatrix} = \begin{bmatrix} F_X \\ 0 \end{bmatrix}$$
$$\begin{bmatrix} X_X & Y_X \\ X_Y & Y_Y \end{bmatrix}\begin{bmatrix} H_{YX} \\ H_{YY} \end{bmatrix} = \begin{bmatrix} 0 \\ F_Y \end{bmatrix} \tag{9}$$

where X_Y is the *Fourier transform* of the seal and housing displacement in the X direction due to an impact load in the Y direction, etc. Equations (9) represent 4 independent equations with 4 unknowns, $(H_{ij})_{i,j=X,Y}$, easily found using Cramers' rule. As noted above, the impedances are general functions of frequency and follow typical formulations for linear systems. The parameters of the system, $\{M,K,C\}_{i,j=X,Y}$ are determined by curve fitting of the discrete impedances $\{H_{ij}\}$ over a certain range of frequencies. The real part of a impedance is modeled as a quadratic polynomial, $Re(H) \sim K - M\omega^2$, and from which the system stiffness and inertia coefficients are obtained. The imaginary part of a impedance is represented as a first order polynomial or straight line, $Im(H) \sim \omega C$, and whose slope renders the damping coefficient. The quality and certainty of the identified system parameters depends on the goodness of the fit over the selected frequency range. Of course, the linearity of the system response and the invariance of the force coefficients with frequency must also be accounted for in the procedure.

The system impedances, $(H_{ij})_{i,j=X,Y}$, are valid for the entire frequency spectrum and only limited in practice by instrumentation and methodology. In the current tests, the accelerometers are only calibrated to a low value of 10 Hz. However, the measured accelerations are not used in the current procedure since it is

verified in the frequency domain that $\ddot{X}=-\omega^2 X$. Furthermore, it is found in the procedure that subtracting the housing inertia force, $(-M_h x \ddot{X})$ degrades the quality of the curve fit for the real portion of the impedances. Therefore, the identification method is valid for the lowest measurable frequency (0.81 Hz). The measurements at exactly 0 Hz are not useful due to a small dc offset (drift) from the transducers. The upper limit of the frequency range is determined by the frequency range excited by the impact gun. The seal displacement frequency response extends up to about 90 Hz for gun excitations with a soft tip. Therefore, the frequency domain curve fitting is performed in the frequency range of 1-90 Hz. However, the experimental discrete impedances (especially the imaginary portion) show considerable scatter for such a wide frequency range. Thus, identification of the slope (damping coefficient) of the imaginary portion becomes too inaccurate. Therefore, in the present procedure, the method described is valuable to identify preliminary seal parameters. These seal coefficients are adjusted when reproducing the system (output/input) transfer functions.

System transfer functions (output/input) are used to obtain more precise measurements of the annular seal force coefficients. The measurements indicate that the cross-coupled impedances are two orders of magnitude smaller than the direct impedances, and hence, their values are within the experimental uncertainty. In a modified identification procedure these impedances are set equal to zero, i.e. $H_{XY}=H_{YX}\approx 0$. No effort is made to identify seal inertia force coefficients $\{M_{ij}\}_{i,j=X,Y}$ since these coefficients are typically small due to the low density of the fluid (air) flowing through the annular seal element. These arguments lead to evaluation of the magnitude of the system (direct) transfer functions as,

$$TF(X_X)=|X_X/F_X|=1/|H_{XX}|=\{(K_{XX}+K_{hX}-\omega^2 M_h)^2+(C_{XX}+C_{hX})^2\omega^2\}^{1/2}$$
$$TF(Y_Y)=|Y_Y/F_Y|=1/|H_{YY}|=\{(K_{YY}+K_{hY}-\omega^2 M_h)^2+(C_{YY}+C_{hY})^2\omega^2\}^{1/2} \quad (8)$$

The transfer functions calculated from the experimental data are evaluated and analytical transfer functions using the preliminary estimates for the seal force coefficients are also determined from equations (8). At first, the test and calculated transfer functions are not likely to match very well over the selected frequency range. However, at this point small adjustments to the seal stiffness and damping values in the analytical model quickly lead to a better match between the model and the experimental results.

UNCERTAINTY OF MEASUREMENTS

The measurement uncertainties for displacement, acceleration, force, seal inlet pressure and mass flow rate are given in Table 6. These uncertainties combine the precision uncertainty of the sensors and the uncertainties resulting from the analog to digital conversion. The seal inlet pressure defines the *pressure ratio* (P_{supply}/P_{amb}), and since the seal discharges to atmospheric conditions (14.7 psia), the uncertainty of the test *pressure ratio* is only 0.3%. The uncertainty for mass flow rate corresponds to that of the turbine flow meter.

Table 6 - Transducer uncertainties

Transducer	Uncertainty
Displacement	± 2.0 μm (0.08 mils)
Acceleration	± 0.001 g
Force	± 0.04 N (0.009 lb)
Seal inlet pressure	± 0.34 MPa (0.05 psi)
Mass flow rate	± 0.0006 kg/sec (0.001 lb/sec)

The uncertainties for displacement and force measurements are only valid for single sample experiments in the time domain. However, the stiffness and damping coefficients are identified in the frequency domain. Thus, magnitudes of uncertainty for the estimated force coefficients must be obtained from a method which transforms the time domain measurement uncertainties to the frequency domain.

In the procedure devised, two sets of time domain signals are necessary. First, an impulse force and associated displacement time response for known values of force coefficients are generated using well known formulae for a 2nd order mass, spring and damper linear system. A second set of derived responses is generated using an impulse force whose original value is lowered by one magnitude of force uncertainty, and a displacement response taken as the superposition of the original response and one magnitude of displacement uncertainty. The original and derived time responses are brought into the frequency domain, and the parameter identification method (described earlier) determines the system impedances; and from these, stiffness and damping coefficients are identified over a certain frequency range . The difference between the original magnitudes of stiffness and damping coefficients and the values identified from the second set of responses reveals the measurement uncertainty for both force coefficients. As expected, the uncertainties vary with the magnitude of the original parameters. The largest uncertainty magnitudes for the stiffness and damping coefficients are equal to 6 KN/m and 20 N sec/m, respectively. *Appendix A* details the analysis performed to estimate the uncertainty of the identified parameters.

COMPUTATIONAL BULK-FLOW MODEL FOR PREDICTIONS

The experimental results demonstrate a peculiar behavior for the seal direct stiffness coefficients which drop sharply for pressure ratios in the range of 1.5 to 2.0. Force coefficients from a bulk-flow model (San Andrés, 1992) accounting for fully developed turbulent flow within the seal predict poorly the measurements. At first instance, it is thought that choked or sonic flow conditions prevail for the test conditions. Table 7 lists typical flow rates from the measurements and estimated Mach number and axial flow Reynolds number at the seal exit.

Table 7. Axial flow Reynolds and Mach numbers at seal exit.
Tests for centered seal, no rotation

Pressure ratio $P_{supply}/P_{ambient}$	Flow rate $\dot{m}$ [kg/s]	Axial Reynolds number $Re_a=\dot{m}/\pi\mu D=\rho V_z c/\mu$	Exit Mach number $Me=V_z/a$,
1.25	0.0070	975	0.22
2.00	0.0145	2,019	0.456
3.00	0.0272	3,788	0.86

where $a=(\gamma R_a T)^{1/2}$=349 m/s is the air sound speed at 21°C, γ=1.4, R_a=286.9 J/kg°K
and air properties, ρ=1.2 kg/m^3, μ=1.8 10^{-5} Pa-s.
seal: D=127 mm, c=0.190 mm

The variation of the axial Reynolds number indicates that the flow conditions within the seal may correspond to operation in the transition regime from laminar to turbulent flow conditions. On the other hand, the exit Mach number is less than 0.5 for pressure ratios below 2.0, and rises as the supply pressure increases. Operation close to sonic conditions are of importance for pressure ratios above 3.0.

Traditional models for predicting force coefficients account for only laminar and/or turbulent flows, and simplify the flow in the transition regime by extending turbulent friction factor lines to the onset of transition flow. Zirkelback and San Andrés (1996) introduce an analysis for the prediction of the dynamic forced response for annular seals in the transition regime to flow turbulence. The model establishes a heuristic curve fit connecting the laminar friction factor to Moody's turbulent friction factor curve in the transition regime from laminar to fully developed turbulent flows. The equations governing the bulk-flow for small amplitude rotor motions about an equilibrium position are solved with a universal friction factor valid for all regimes. The measured flow rates and extracted force coefficients are compared to predictions

based on the computer program of Zirkelback and San Andrés (1996). The transition zone from laminar to turbulent flow is defined in the range, $1{,}000<Re_a<3{,}000$.[1]

TEST RESULTS AND DISCUSSION

Experiments are conducted for pressure ratios ($P_{supply}/P_{ambient}$) ranging from 1.25 to 3.0 without journal rotation and at a shaft speed of 3,600 rpm. A set of tests is also conducted for the seal statically off-centered to 50% of the radial clearance and without shaft speed. All tests are performed for air at a temperature of ~ 21°C (70° F) and discharging to atmospheric conditions. Note that the experimental measurements demonstrate little cross-coupling, i.e. $K_{XY}=K_{YX}=C_{XY}=C_{YX}=0$ for the annular seal, and the inertia coefficients are regarded as negligible in the identification procedure, i.e. $\{M_{ij}=0\}_{ij=X,Y}$. For centered conditions, the predictions show the direct coefficients to be identical, i.e. $K_{XX}=K_{YY}$, and the cross-coupled coefficients to be anti-symmetric, i.e. $K_{XY}=-K_{YX}$.

Table 8 lists the identified seal force coefficients and uncertainties for each test. In all cases, the measured structural stiffness and damping are subtracted so that the tabulated coefficients represent the seal contribution only. Table 9 lists values and uncertainties for the inlet air temperature, roller bearing lubricant temperature, housing pressure, air line pressure before and after flow meters, and mass flow rate. Mass flow rate measurements with the visual meter are noted by an (*). All other mass flow measurements correspond to the turbine flow meter.

Results and predictions for centered seal without rotation

Figure 4 depicts the measured seal mass flow rate, and seal direct stiffness (K_{XX},K_{YY}), and direct damping (C_{XX},C_{YY}) coefficients as functions of the pressure ratio across the seal for a centered seal without shaft rotation. The figures depict bars denoting the uncertainty in the measurements. The largest possible uncertainty magnitudes of 6 kN/m and 20 N-sec/m are displayed for the stiffness and damping coefficients, respectively.

The measured mass flow increases steadily with the pressure ratio and agrees well with the numerical predictions. The (identified) seal direct stiffness coefficients (K_{XX},K_{YY}) are nearly identical, and the experiments demonstrate the test seal clearance to be uniform around the seal journal. The error bars on each test result indicate the measurement uncertainty in the evaluation of the seal stiffness. The seal direct stiffness decreases and it even becomes negative as the pressure ratio increases from 1.25 to 2.00. For increasing pressure ratios above 2.0, the stiffness appears to increase slightly and then levels-off. The predictions show the same trend as the test measurements with a dip in stiffness at a pressure ratio equal to 2.0. For pressure ratios above 2.5 the predictions show increasing magnitudes of stiffness but the test results show an opposite behavior. Note that predictions based on a bulk-flow model without a transition zone will not have predicted the drop in stiffness but rather a continuous increase with supply pressure.

The test and predicted seal direct damping coefficients (C_{XX},C_{YY}) correlate well for most pressure ratios. Note however that the measurements estimate larger damping coefficients for certain pressures. The trend of the damping coefficients is to increase with the raises in pressure supply (due to increased dissipation and turbulence), and do not show the peculiar behavior of the stiffness coefficients.

Results and predictions for a centered seal with shaft rotation to 3,600 rpm

Figure 5 shows the measured seal mass flow rate, and identified seal direct stiffness (K_{XX},K_{YY}), and direct damping (C_{XX},C_{YY}) coefficients as functions of the pressure ratio for a centered seal with shaft rotation at 3,600 rpm. The measured mass flow rates agree well with the predictions, and do show approximately a

---

[1] The predictions are calculated with a seal inlet loss coefficient $\xi=0.20$ and no exit pressure recovery factor. The seal surfaces, although originally smooth, are accounted as rough with a surface roughness ratio equal to 0.05. This value attempts to account for a thin film of oil debris that built up in the seal surfaces and due to lack of appropriate filtering in the air lines.

20% reduction if directly compared to the mass flow rate values for the no rotation tests. The axial flow Reynolds number ranges from 1,500 to 3,970 in these tests.

The direct stiffness coefficients (K_{XX},K_{YY}) exhibit the same peculiar behavior as for the measurements made without shaft rotation. It is still apparent that in the range of pressure ratios of 1.50 to 2.00, the direct stiffness decreases, and from 2.00 to 2.50 the stiffness increases. Also, between pressure ratios of 2.5 and 3.0, there is little change in direct stiffness. The predictions show the same behavior as for the centered seal case and no rotation. The measurements demonstrate that shaft rotation has very little effect (if any) on the direct stiffness of the seal. Note that theory largely overestimates the direct stiffness at a pressure ratio of 3.00. The direct damping coefficients (C_{XX},C_{YY}) show a steady increase for increasing pressure ratios. The theoretical model agrees well with the measured direct damping for the range of pressure ratios tested.

Results and predictions for an off- centered seal without shaft rotation

In these tests the seal is displaced off-center in the X direction to 50% of the radial clearance, and experiments are carried out for pressure ratios equal to 1.0, 2.0 and 2.5. Figure 6 depicts the measured seal mass flow rate, and identified seal direct stiffness (K_{XX},K_{YY}), and direct damping (C_{XX},C_{YY}) coefficients as functions of the pressure ratio. The measured mass flow rates increase steadily with pressure ratio and are slightly lower than the computed predictions. The axial flow Reynolds number ranges from 1,500 to 2,870 in these tests.

The direct stiffness (K_{XX},K_{YY}) behave differently with increasing pressure ratios. The stiffness (K_{XX}) increases from a pressure ratio of 1.50 to 2.00, and then drops dramatically for a pressure ratio of 2.50. The other direct stiffness (K_{YY}) decreases from a pressure ratio of 1.50 to 2.00 and does not change with increasing pressure ratios. The computed predictions correlate very poorly with the identified seal stiffness coefficients. It is noted that for a pressure ratio equal to 2.50 the seal is nearly unstable, in the sense that small forces produce very large seal displacements. For a pressure ratio equal to 3.00, the test system undergoes through a self-exciting phenomena with seal motions knocking the clearance even without an external force excitation. At this particular test condition it is believed that choked flow conditions exist on the portion of the seal with the smallest clearance. Unlike the direct stiffness measurements, the direct damping coefficients do not show a marked difference for the off-center seal condition. Both direct damping coefficients (C_{XX},C_{YY}) increase with increasing pressure ratios and agree well with the computed predictions.

Test system transfer functions

Figure 7 and 8 show the magnitude of the system transfer functions (TF) for displacements in the X and Y direction due to impact loads in the same directions. These transfer functions are the averages of 32 impact tests, and include the housing mass (M_h) and structure stiffness and damping $\{K_{hi},C_{hi}\}_{i=X,Y}$ coefficients. The top Figure (7a) shows the transfer functions for pressure ratios of 1.00, 1.25, and 1.50, while the bottom Figure (7b) displays the transfer functions for pressure ratios 1.75, 2.00, 2.25, 2.50 and 3.00. Note that the value of transfer function close to zero frequency indicates (in a linear model) the value of the system flexibility, *i.e.* $1/K_X$ *or* $1/K_Y$, while the peak magnitude (TF) at the damped natural frequency is proportional to the amount of damping in the system. The following observations are made in regard to the measured results. Since the mass of the system is regarded as constant, i.e. M_h=10 kg, large changes in the natural frequency of the seal and housing structure are most likely related to changes in the stiffness of the seal (for sufficiently small amounts of damping). Note that the test at a pressure ratio equal to one (1.0) indicates no forced air flow through the seal, and shows the characteristic (TF) of a second order system $\{K,C,M\}$.

The system natural frequency increases for pressure ratios increasing from 1.00 to 1.25, thus indicating the (stiffening) contribution of the seal as it is pressurized. For the pressure ratios equal to1.25 and 1.50, the natural frequency does not change significantly, thus suggesting an insignificant change in seal direct stiffness. The system natural frequency drops to nearly zero for pressure ratios equal to1.75 and 2.0 and

the (*TF*)'s show the characteristic response of a first order system *{M,C}*. Larger values of the seal pressure ratio demonstrate an increase in the natural frequency which is accompanied by an increase in the seal direct stiffness coefficients. The second observation is related to the amplitude of the (*TF*) at the damped natural frequency which steadily decreases as the pressure ratio increases, and thus indicates increasing values of the direct damping coefficients. However, exceptions are evident at the pressure ratios equal to 1.75 and 2.00 where it is difficult to determine the actual natural frequency of the test system.

Figure 9 shows typical experimental and curve-fit direct impedances (H_{XX}, real and imaginary parts) for a centered seal without shaft rotation at a pressure ratio equal to 2.50. Symbols denote the extracted impedance from the test measurements and the solid lines represent the curve fits. In the real portion of H_{XX}, the intercept at null frequency indicates the combined stiffness of the seal and housing structure ($K_{XX}+K_{hX}$). The quadrature in the solid line represents the housing mass (M_h). The slope of the imaginary part of H_{XX} represents the combined seal and housing damping ($C_{XX}+C_{hX}$) coefficient. The linear model with uniform stiffness and damping coefficients represents well the measurements, although the scatter in the imaginary part of H_{XX} appears to be too large. Figure 10 shows typical time domain responses, x(t), due to an impact load in the same direction. The test conditions are identical as those given for the results in Figure 9. Note the different time scales for display of the impact load and seal dynamic forced response. The impact lasts approximately 5 msec, while the seal forced response extends well above 150 msec.

Coherence of the experimental measurements

Figures 11 and 12 show the coherence of the seal displacements and accelerations to 32 impacts for the off-center seal case without shaft rotation and at a pressure ratio equal to 2.50. Note that these experiments show perhaps the worst correlation between input load and output response due to the close proximity to sonic flow conditions. Figure 11a shows the coherence of the displacement (X) due to an impact in the same direction (F_X). Certainly, the displacement in the X direction correlates strongly to the impact in the same direction. Inspection of Figure 11b shows that the displacement (Y) is not related to the impacts (F_X). This suggests that either the seal does not exhibit any cross-coupling or the Y displacement sensor is not operating properly. Figure 11c shows the coherence of the acceleration (A_X) relative to the impact (F_X). The coherence below 10 Hz is not acceptable since the accelerometer is not calibrated for measurements below this frequency. Figure 11d shows poor coherence between the acceleration (A_Y) relative to impacts (F_X), demonstrating no cross-coupling effects. Figure 12 shows similar results with excellent coherence for the ratios of displacement and acceleration in the Y direction due to impacts in the same direction, (F_Y). Here, cross-coupled effects are also minimal.

Figures 13 through 26 show the measured transfer functions *(TF)* and the analytical transfer functions for each test condition. The analytical transfer functions (curve fit) are given by equations (8). In all figures the symbols represent test values while solid lines denote the curve fits. Figures 13 through 19 show the *(TF)* for the tests with a centered seal and no shaft rotation. In general the analytical *(TFs)* match the experimental data well. The worst agreement is for a pressure ratio equal to 1.75 (Figure 15). In this case, it is difficult to indicate if in fact the damped natural frequency is at the peak shown by the curve fit, or perhaps the stiffness is absent, in which case the natural frequency is essentially zero.

Figures 20 through 22 show the transfer functions for the tests with an off-center seal and no shaft rotation. The curve fits for all three pressure ratios fit the experimental data well.
Figures 23 through 26 show the transfer functions for the tests with a centered seal and shaft rotation at 3,600 rpm. The influence of shaft runout when rotating is apparent in all test results at the frequency of 60 Hz. Although the analytical *(TF)* model does not simulate the synchronous response to shaft rotation, it matches the experimental data well.

CONCLUSIONS

Dynamic force coefficients for a smooth surface, annular seal with a uniform clearance are identified experimentally for increasing air pressure supplies and for operation without rotation and at 3,600 rpm. The

seal element is of length, diameter, and clearance equal to 40.6 mm, 127 mm, and 0.190 mm, respectively. Impact guns excite the test seal in two orthogonal directions and transfer functions for the seal displacements and accelerations are recorded in the frequency domain. Averaged frequency responses of 32 impacts are used to determine the test system impedance coefficients and to extract the seal force stiffness and damping coefficients from transfer functions.

The experiments demonstrate the test seal has no cross-coupling effects. The seal flow rate and direct damping coefficients increase with increases in the supply pressure and show little variation with the shaft rotational speed. Estimations of the axial flow number indicate operation in the transition regime from laminar to turbulent flow conditions. The test direct stiffness coefficients vary greatly with the pressure supply and present a dramatic drop for a supply pressure twice the value of ambient pressure. Measurements for an off-centered seal to 50% of its radial clearance are performed to pressure ratios equal to 2.5. Larger values of inlet pressure cause the seal to go unstable due to the onset of choked flow.

Repeated measurements show that the identified direct stiffness and direct damping coefficients are accurate, with uncertainties in the range of 6 KN/m for stiffness and 20 N sec/m for damping coefficients. Numerical predictions based on a bulk-flow model which accounts for transition flow to turbulence agree favorably with the measurements of flow rate and direct damping coefficients. Predictions for direct stiffness coefficients show similar trends as the measurements, although large differences are evident for the largest pressure ratios tested.

ACKNOWLEDGMENTS

The help of Mr. Jeremy Lochte on the experimental work and of Mr. Jiming Li on the evaluation of the predictions is gratefully acknowledged.

REFERENCES

Brockwell, K., Kleinbub, D., and Dmochowski, W., 1990 "Measurement and Calculation of the Dynamic Operating Characteristics of the Five-Shoe, Tilting Pad Journal Bearing," Tribology Transactions, Vol. 33, No. 4, pp. 481-492.

Burrows, C.R. and Sahinkaya, M.N., 1982 "Frequency-Domain Estimation of Linearized Oil-Film Coefficients," Transactions of the ASME, Vol. 104, April, pp. 210-215.

Childs, D.W., Nelson, C.E., Nicks, C, Scharrer, J., Elrod, D., and Hale, K., 1986 "Theory Versus Experiment for the Rotordynamic Coefficients of Annular Gas Seals: Part 1 - Test Facility and Apparatus," Journal of Tribology, Vol. 108, July, pp. 426-432.

Ewins, D.J., 1986 Modal Testing: Theory and Practice, Research Studies Press LTD.

Goodwin, M.J., 1991 "Experimental Techniques for Bearing Impedance Measurement," Journal of Engineering for Industry, Vol. 113, August, pp. 335-342.

Hagg, A.C and Sankey, G.O., 1956 "Some Dynamic Properties of Oil-Film Journal Bearings with Reference to the Unbalance Vibration of Rotors," Journal of Applied Mechanics, Vol. 23, No. 1, June, pp. 302-306.

Lund, J.W., 1987 "Review of the Concept of Dynamic Coefficients for Fluid Film Journal Bearings," Journal of Tribology, Vol. 109, January, pp. 37-41.

Mitchell, L.D. and Elliott, K.B., 1984 "How to Design Stingers for Vibration Testing of Structures," Sound and Vibration, April, pp. 14-18.

Morton, P.G., 1971 "Measurement of the Dynamic Characteristics of a Large Sleeve Bearing," Journal of Lubrication Technology, January, pp. 143-150.

Nelson, C.C., Childs, D.W, Nicks, C., and Elrod, D., 1986 "Theory Versus Experiment for the Rotordynamic Coefficients of Annular Gas Seals: Part 2 - Constant-Clearance and Convergent-Tapered Geometry," Journal of Tribology, Vol. 108, July, pp. 433-438.

Nordmann, R. and Schollhorn, K., 1980 "Identification of Stiffness and Damping Coefficients of Journal Bearings by Means of the Impact Method," Proc. 2nd International Conf. On Vibrations in Rot. Mach., IMechE, pp.231-238.

Parkins, D.W., 1979 "Theoretical and Experimental Determination of the Dynamic Characteristics of a Hydrodynamic Journal Bearing," Journal of Lubrication Technology, Vol. 101, April, pp. 129-137.

Parkins, D.W., 1981 "Measured Characteristics of a Journal Bearing Oil Film," Journal of Lubrication Technology, Vol. 103, January, pp. 120-125.

Parkins, D.W., 1995 "Measurement of Oil Film Journal Bearing Damping Coefficients - An Extension of the Selected Orbit Technique," Journal of Tribology, Vol. 117, October, pp. 696-701.

Qiu, Z.L. and Tieu, A.K., 1993 "Full Determination of Dynamic Coefficients of Fluid Film Bearings from Impulse Responses," Proc. Of 4th ASIA-PACIFIC Vibration Conference, Kitakyushu, Japan, Nov. 14-18, Vol. 2, pp. 527-532.

Rouvas, Constantinos, 1993, "Parameter Identification of the Rotordynamic Coefficients of High-Reynolds-Number Hydrostatic Bearings," Ph.D. Dissertation, Texas A&M University.

San Andrés, L., 1991, "Analysis of Variable Fluid Properties, Turbulent Annular Seals," *ASME Journal of Tribology*, Vol. 113, pp. 694-702.

Stanway, R., 1983 "Identification of Linearized Squeeze-Film Dynamics Using Synchronous Excitation," Proc. Inst. Mech. Eng., Vol. 197C, pp. 199-204.

Swanson, E.E. and Kirk, R.G., 1996 "Survey of Experimental Data for Fixed Geometry Hydrodynamic Journal Bearings," ASME Paper 96-Trib-65.

Tieu, A.K. and Qiu, Z.L., 1994 "Identification of Sixteen Dynamic Coefficients of Two Journal Bearings from Experimental Unbalance Responses," *Wear*, Vol. 177, pp. 63-69.

Zirkelback, N., and L. San Andrés, 1996, "Bulk-Flow Model for the Transition to Turbulence Regime in Annular Seals," *STLE Tribology Transactions, Vol.39*, 4, pp. 835-842.

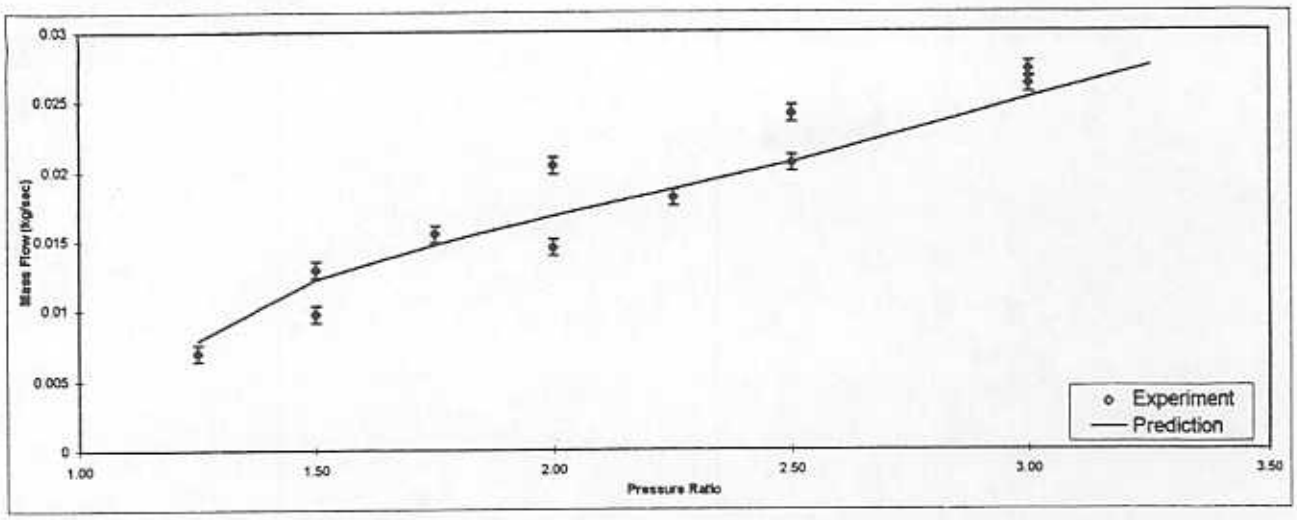

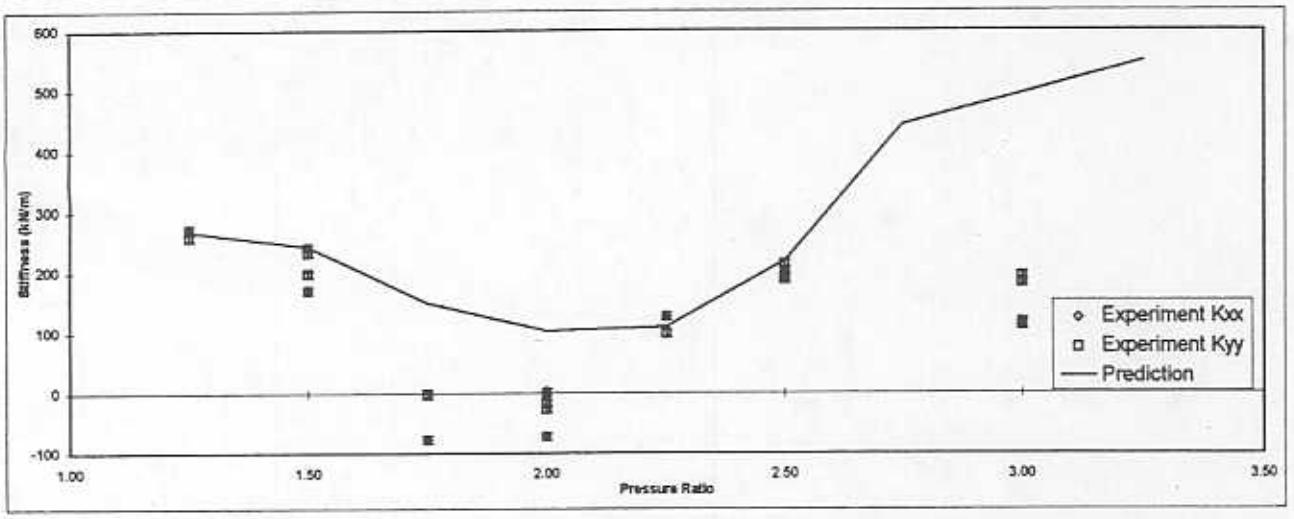

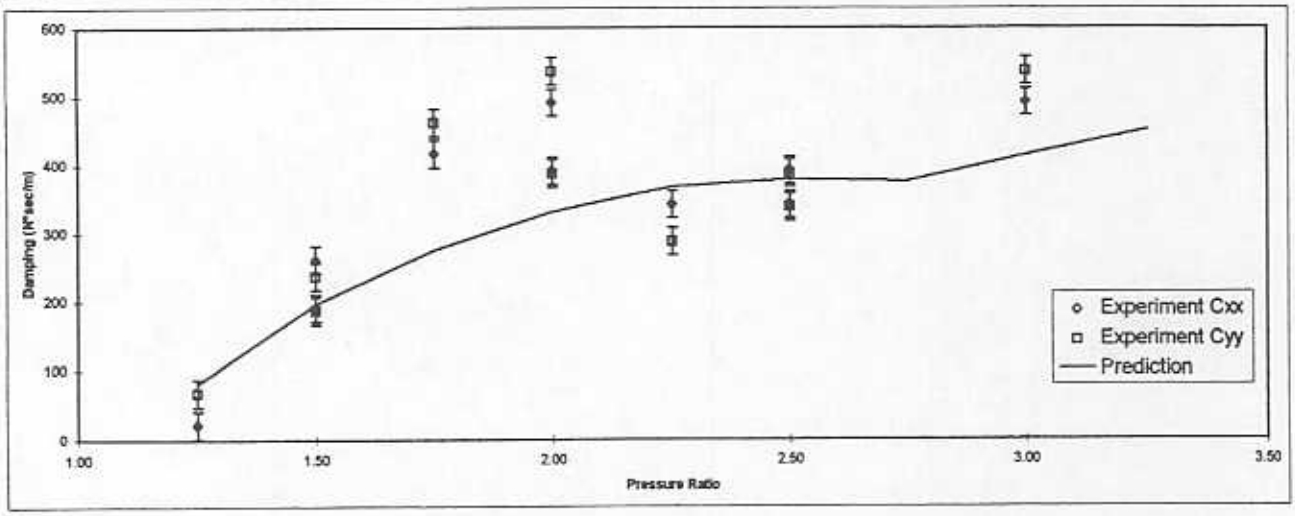

Figure 4 - Seal mass flow, direct stiffness and damping for centered seal and no shaft rotation

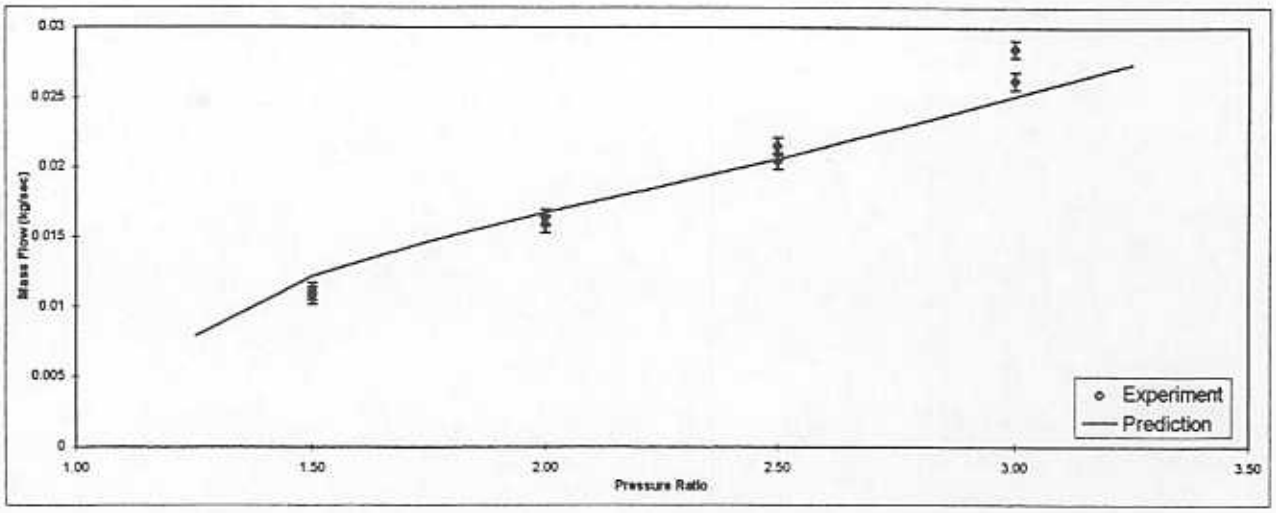

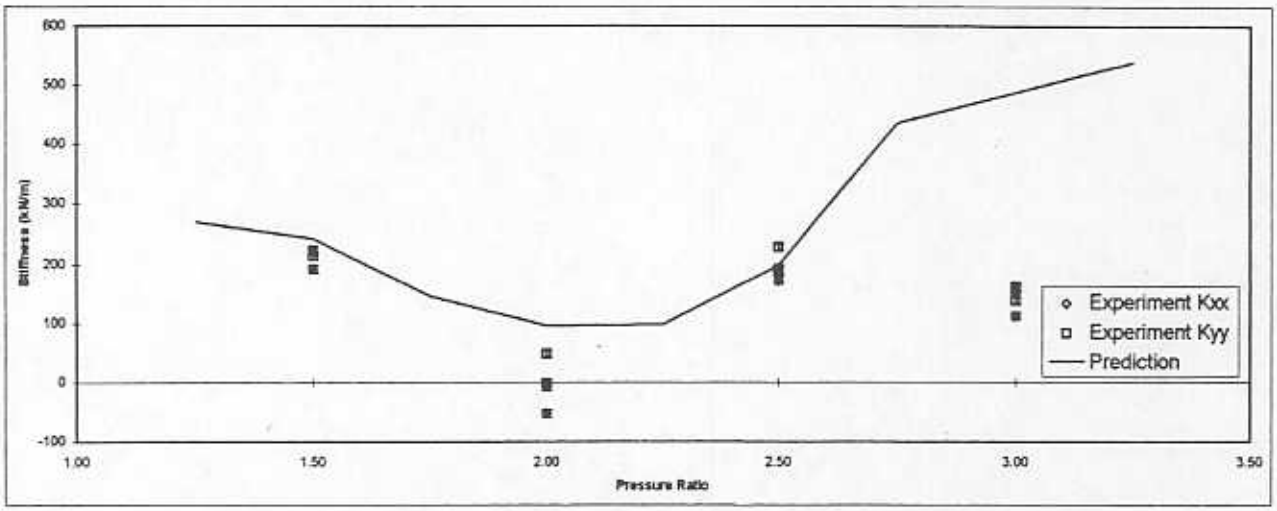

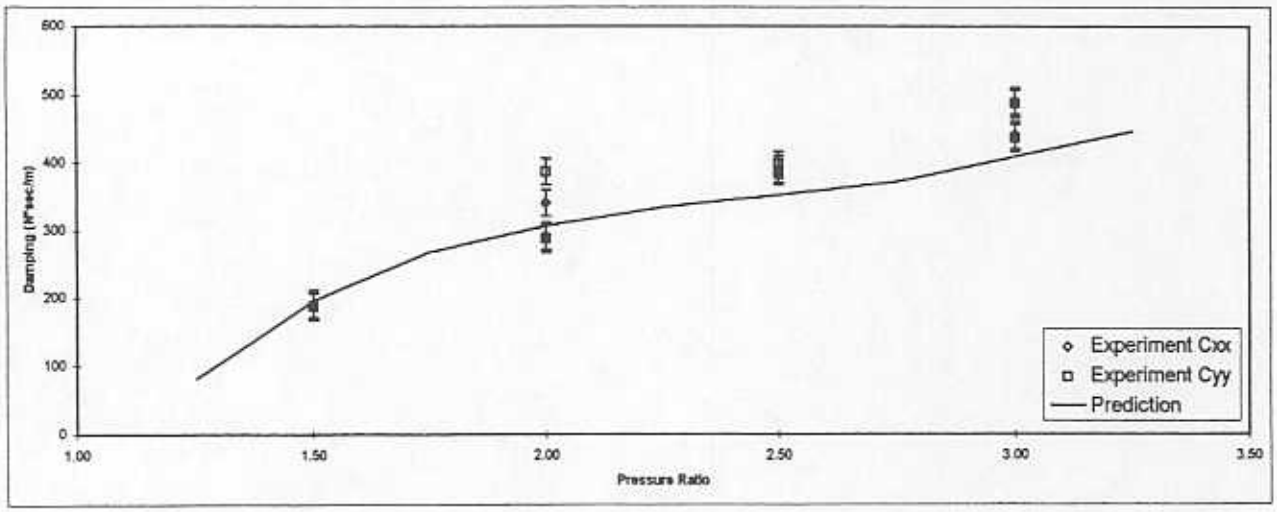

Figure 5 - Seal mass flow, direct stiffness and damping for centered seal and shaft rotation = 3,600 rpm

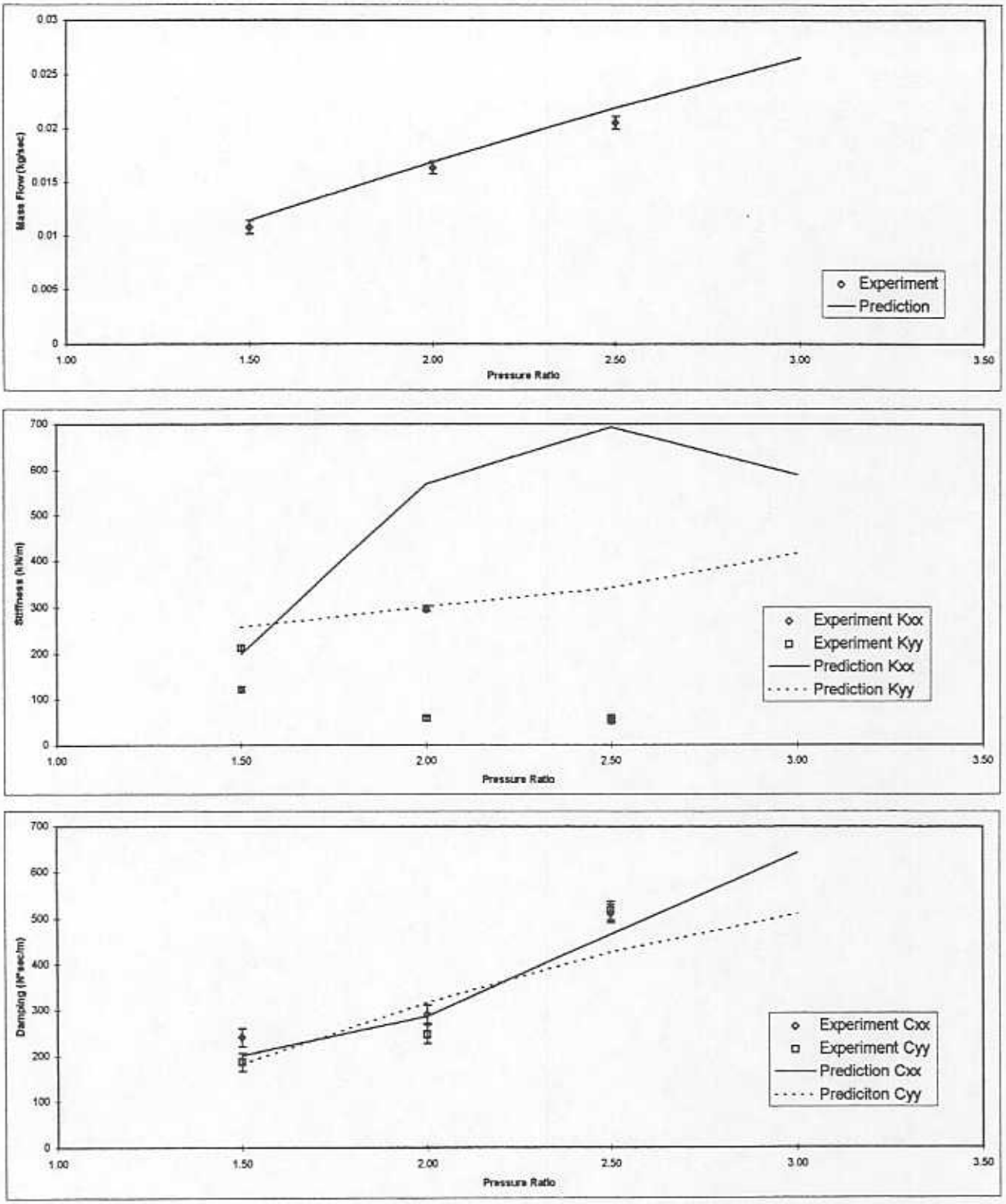

Figure 6 - Seal mass flow, direct stiffness and damping for off-center seal and no shaft rotation

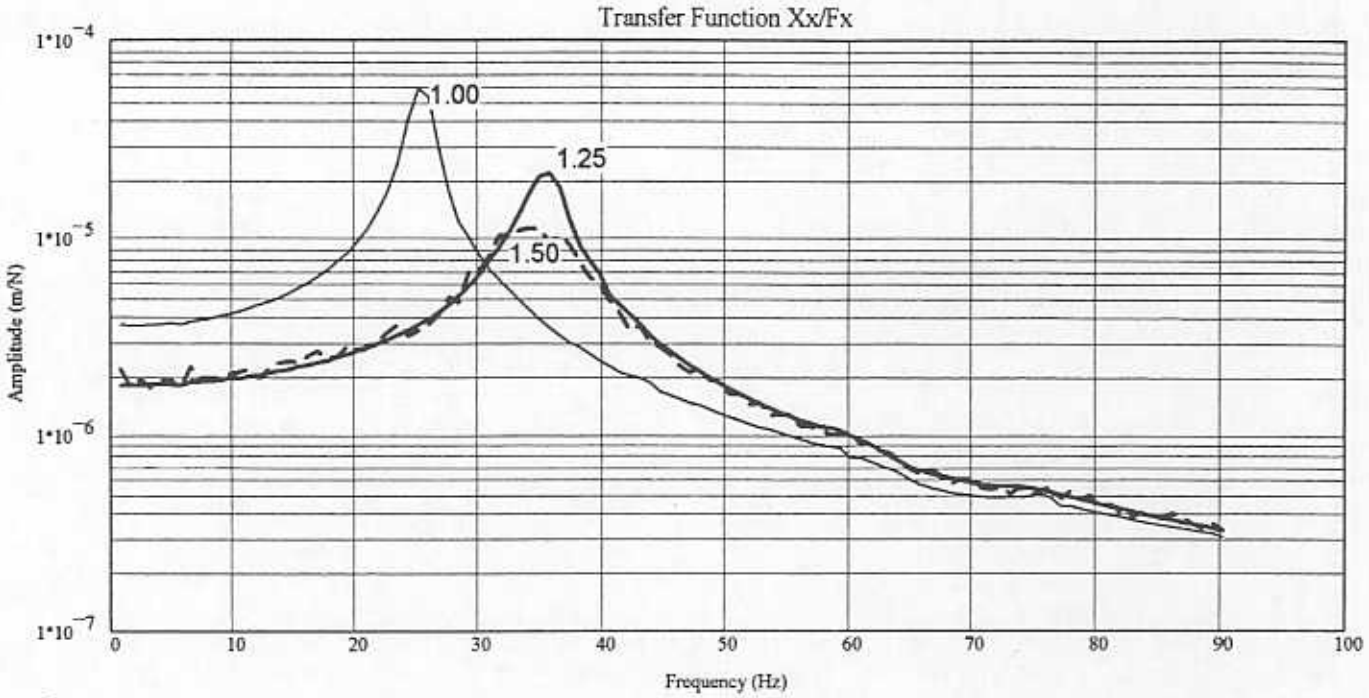

(a)

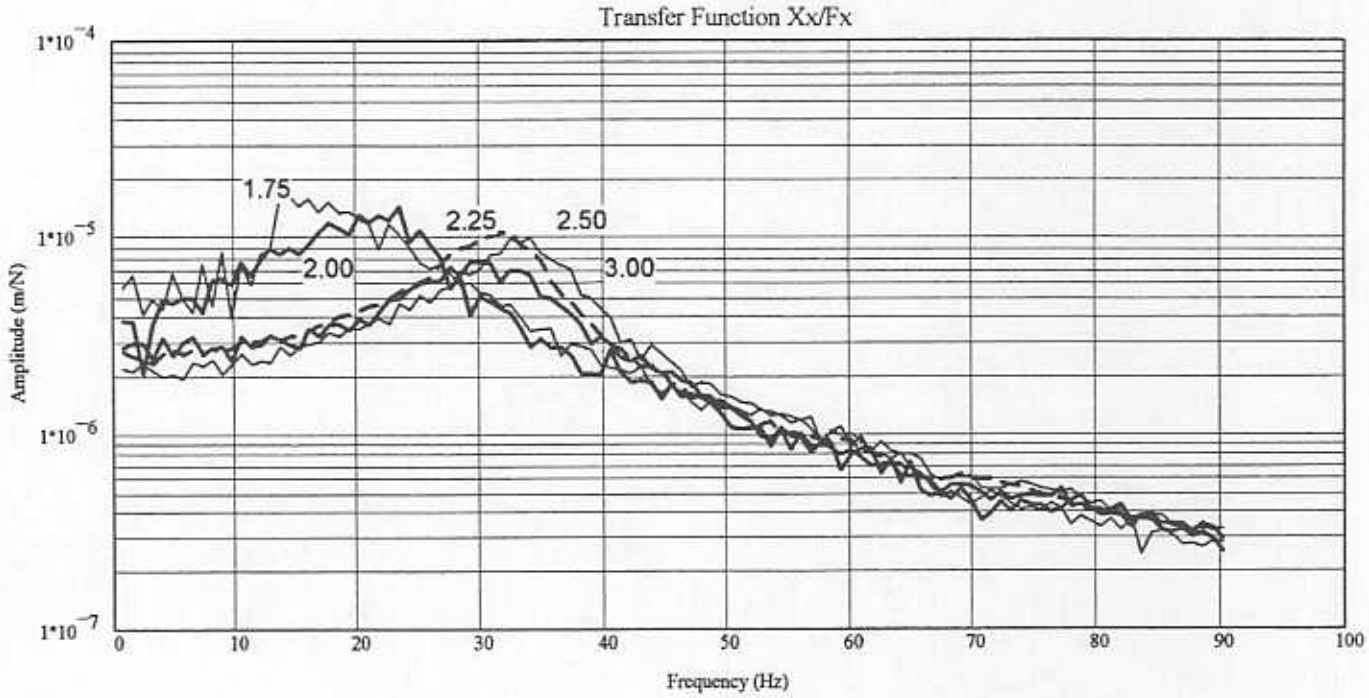

(b)

Figure 7 - Experimental transfer function (Xx/Fx) for centered seal and no shaft rotation. Pressure ratio varies

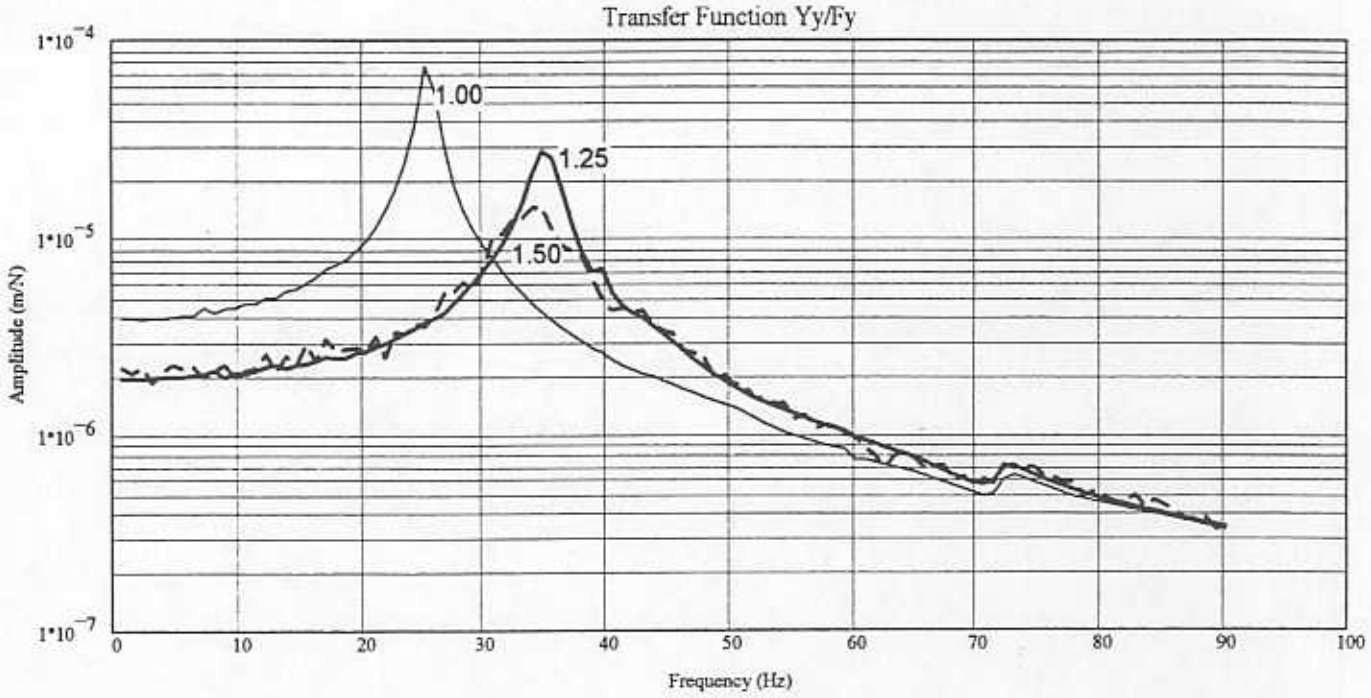

(a)

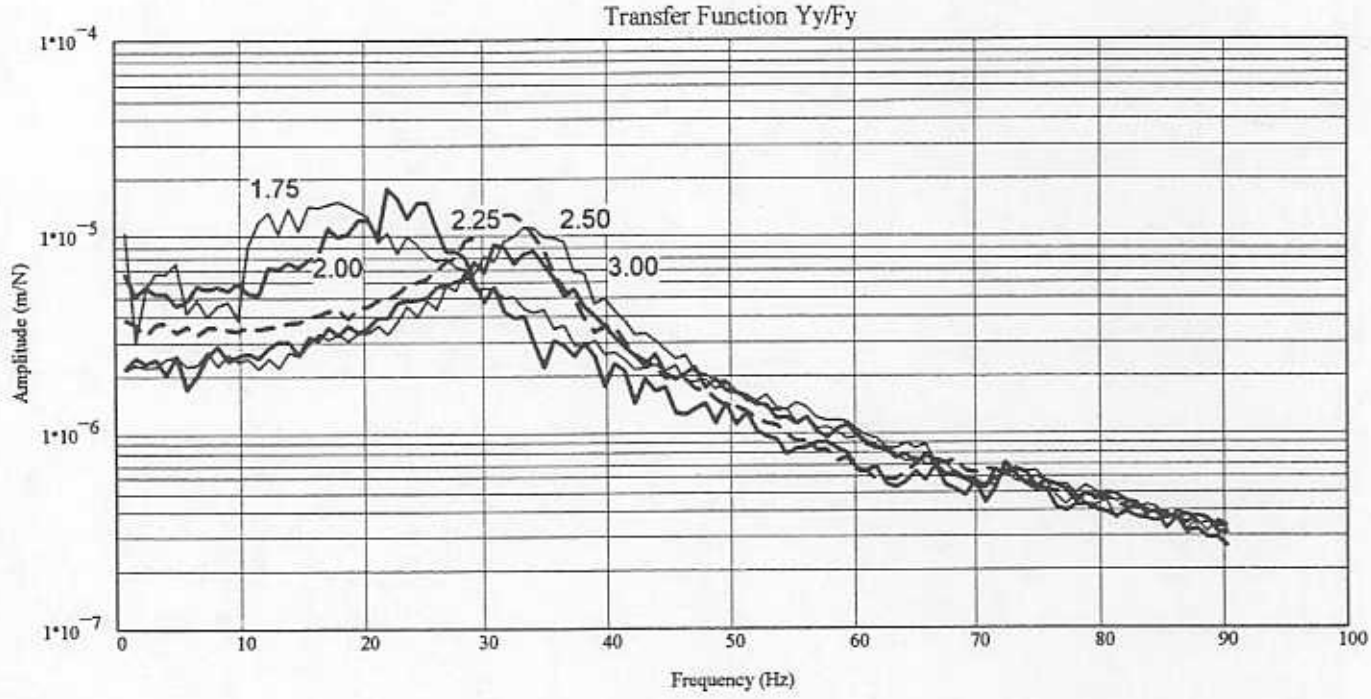

(b)

Figure 8 - Experimental transfer function (Yy/Fy) for centered seal and no shaft rotation. Pressure ratio varies

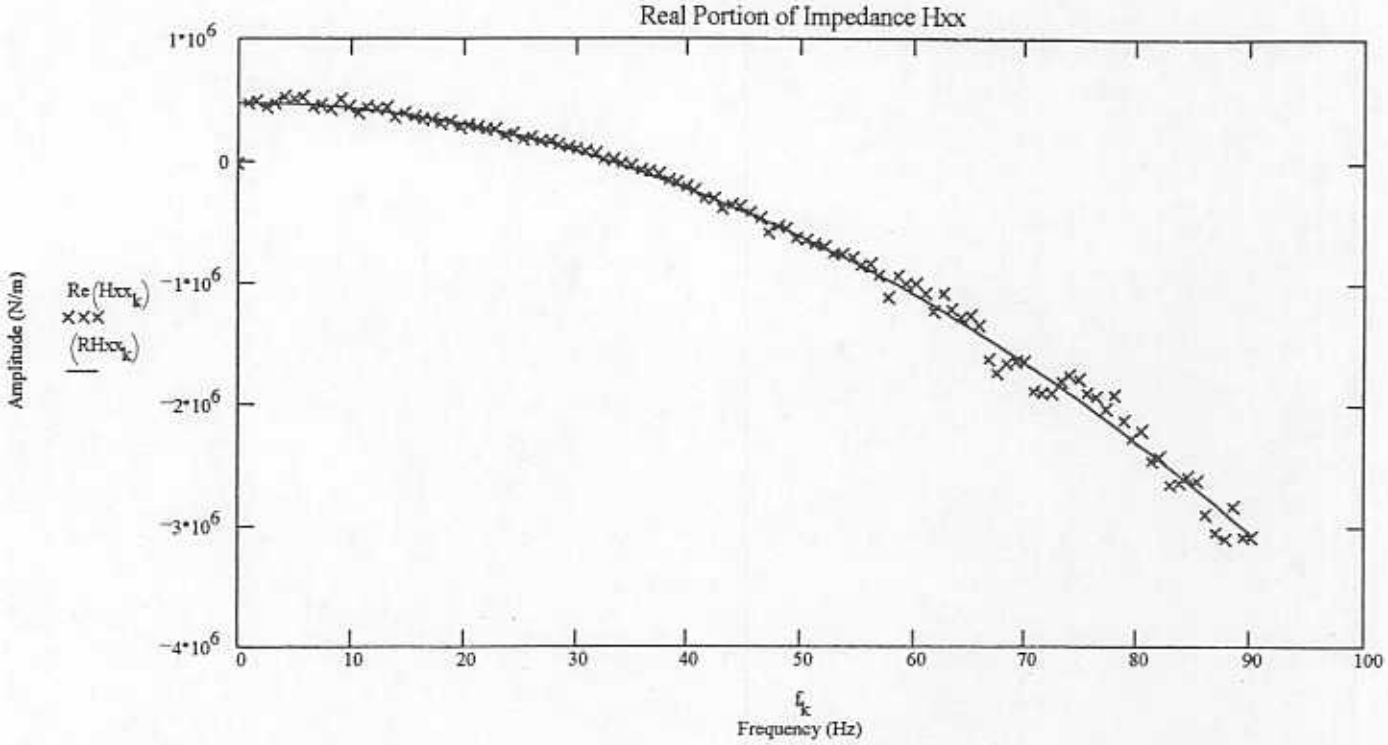

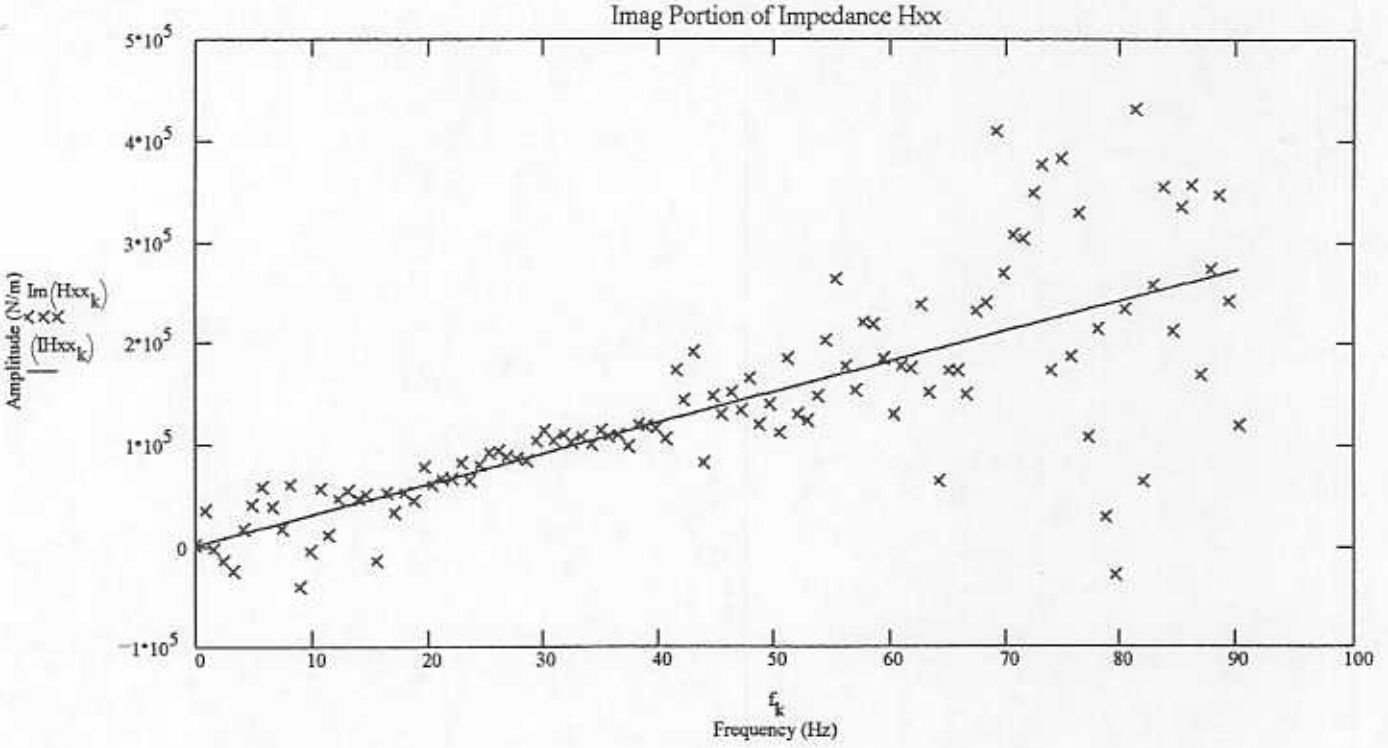

Figure 9 - Impedance (Hxx) for centered seal, no shaft rotation, pressure ratio = 2.5.
Real and imaginary parts

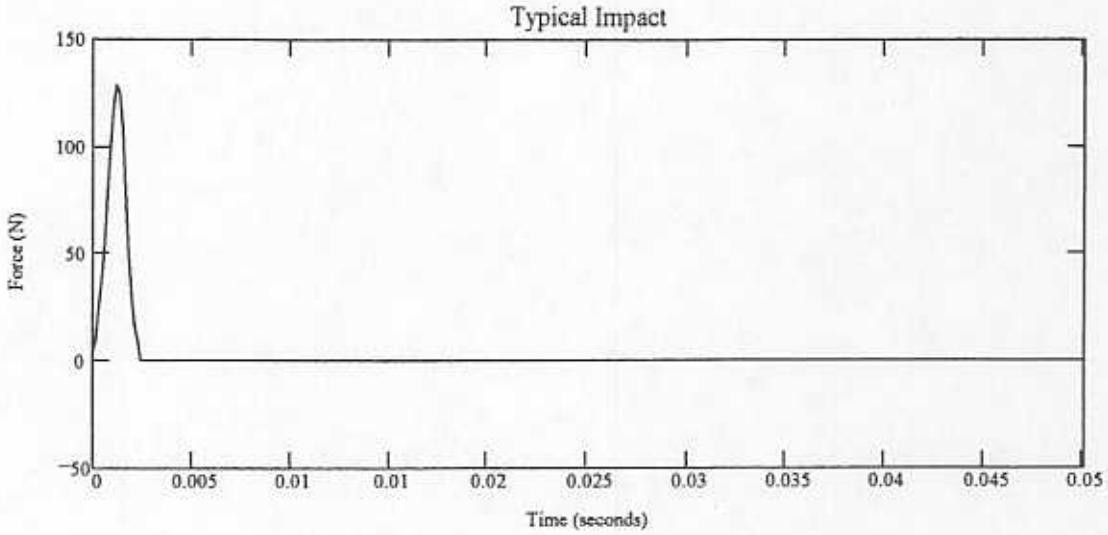

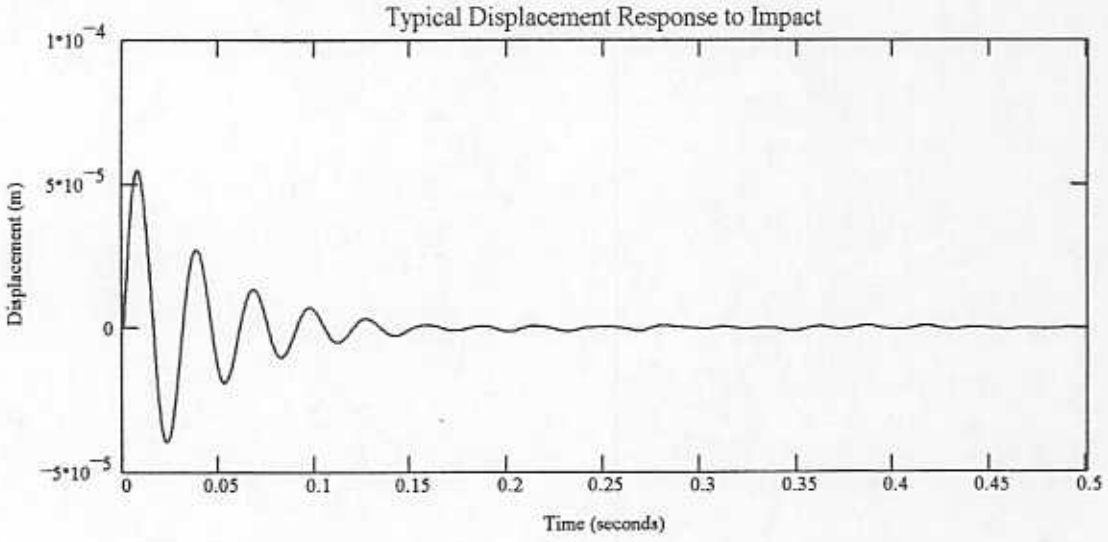

Figure 10 - Time domain impact load and response signals (X direction) for centered seal, no shaft rotation, pressure ratio = 2.5

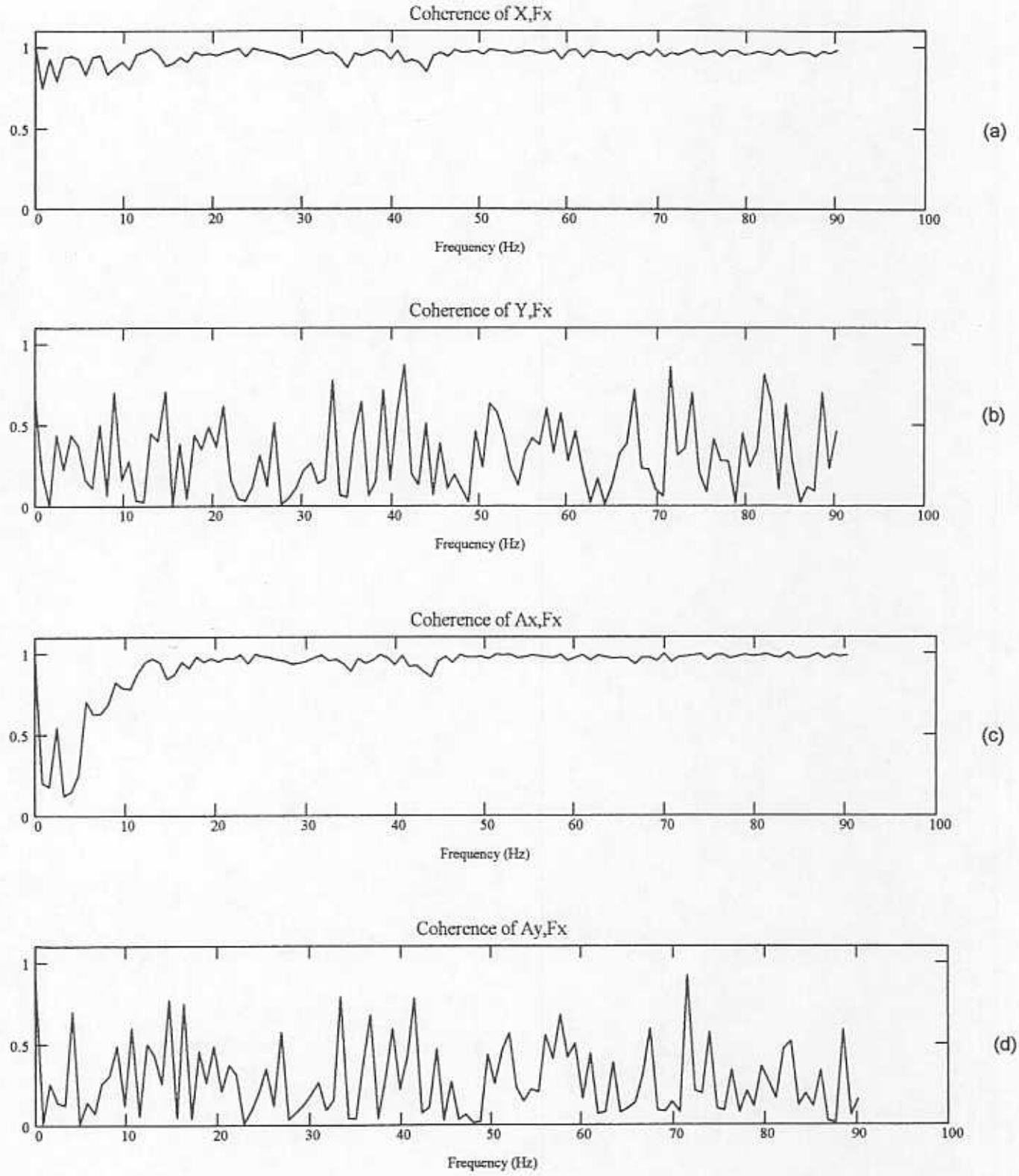

Figure 11 - Coherences for off-center seal, no shaft rotation, pressure ratio = 2.5

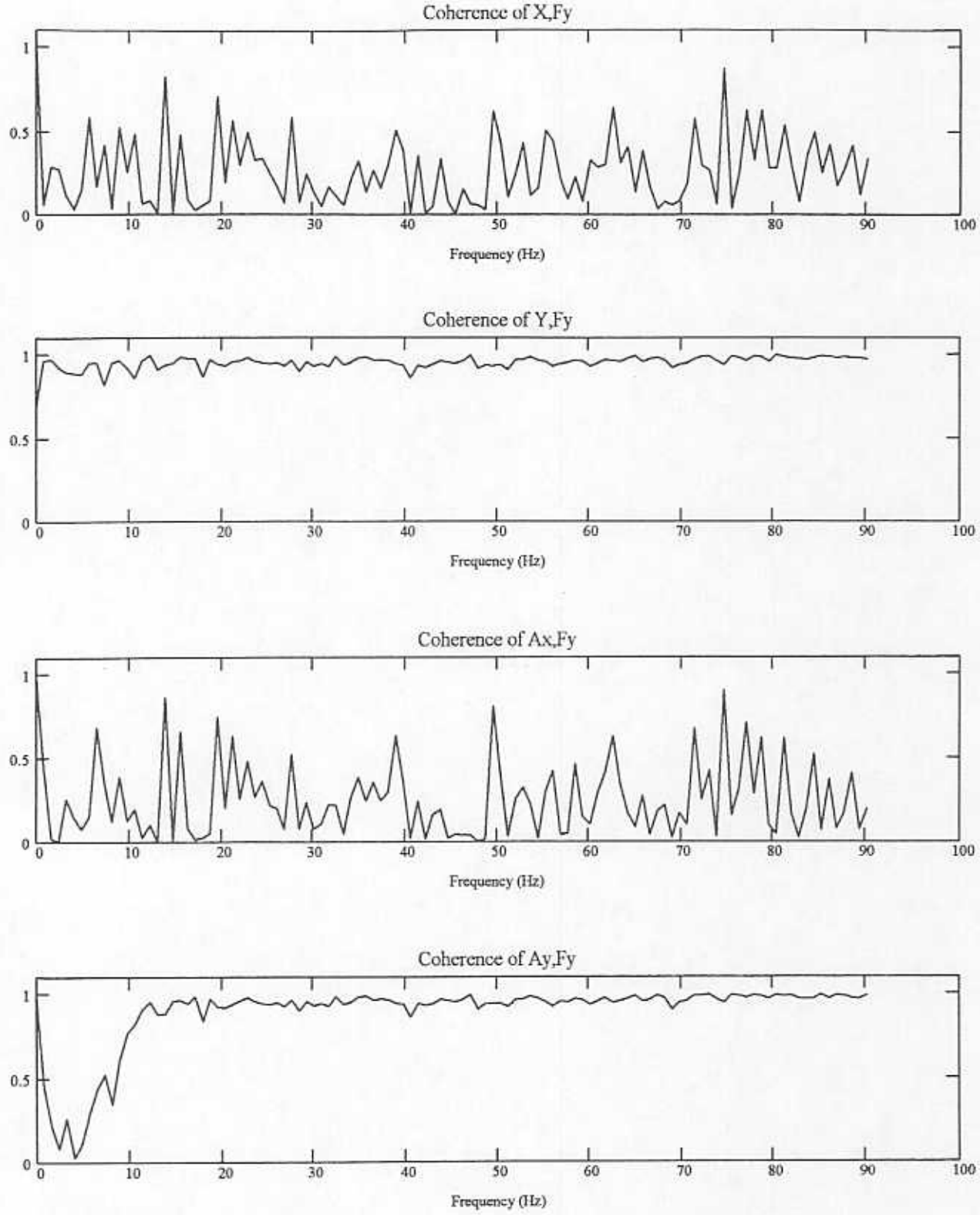

Figure 12 - Coherences for off-center seal, no shaft rotation, pressure ratio = 2.5

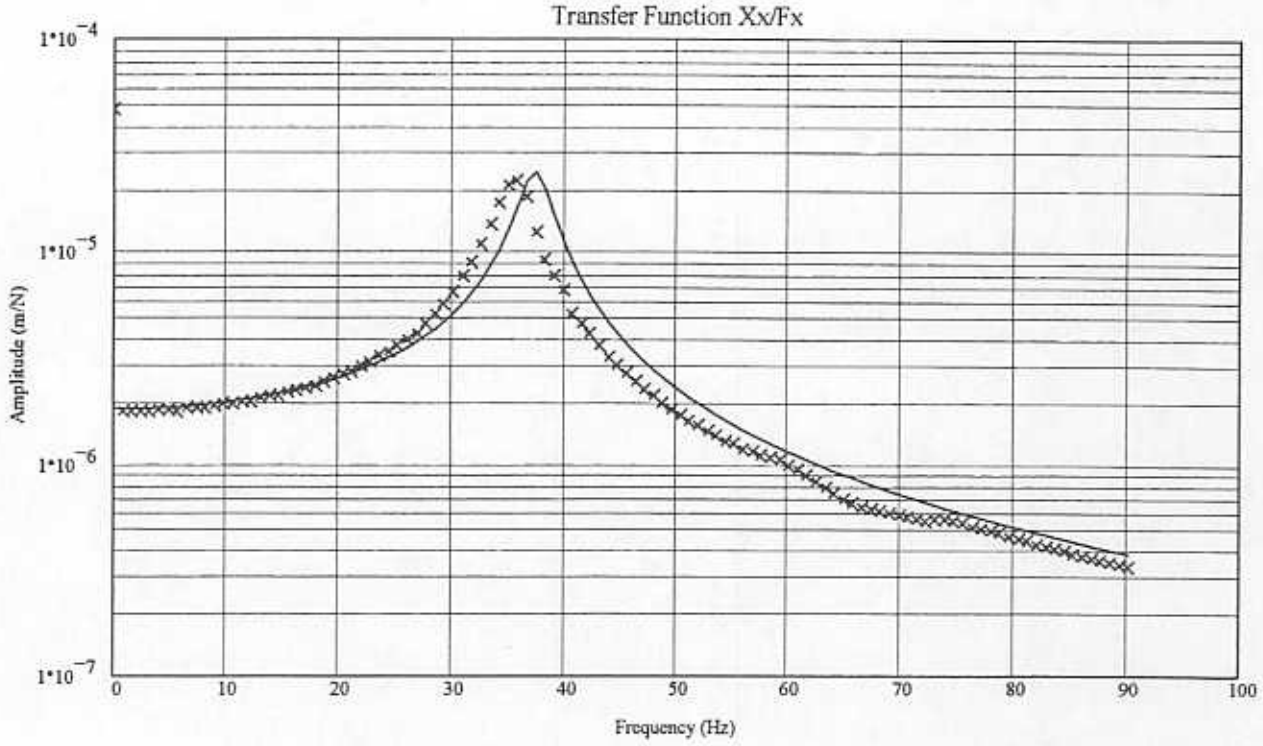

(a)

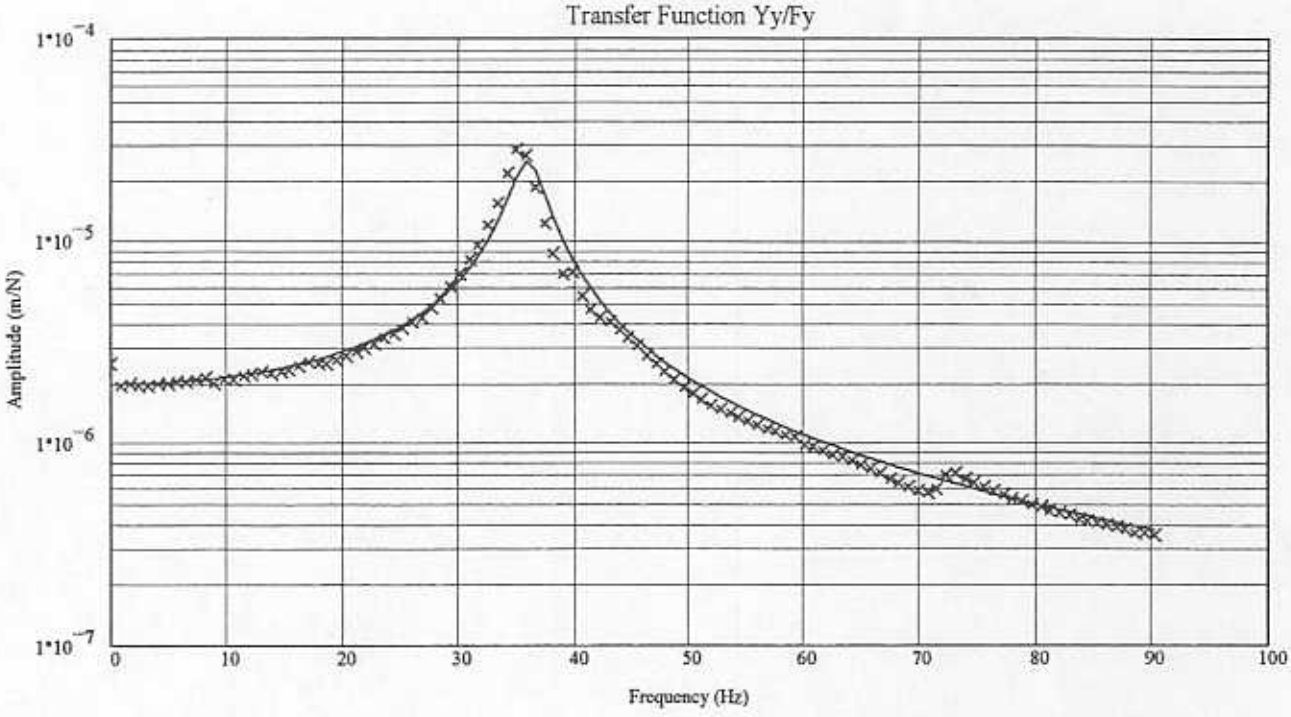

(b)

Figure 13 - Transfer functions for centered seal, no shaft rotation, pressure ratio = 1.25
(symbols = tests, lines = curve fits)

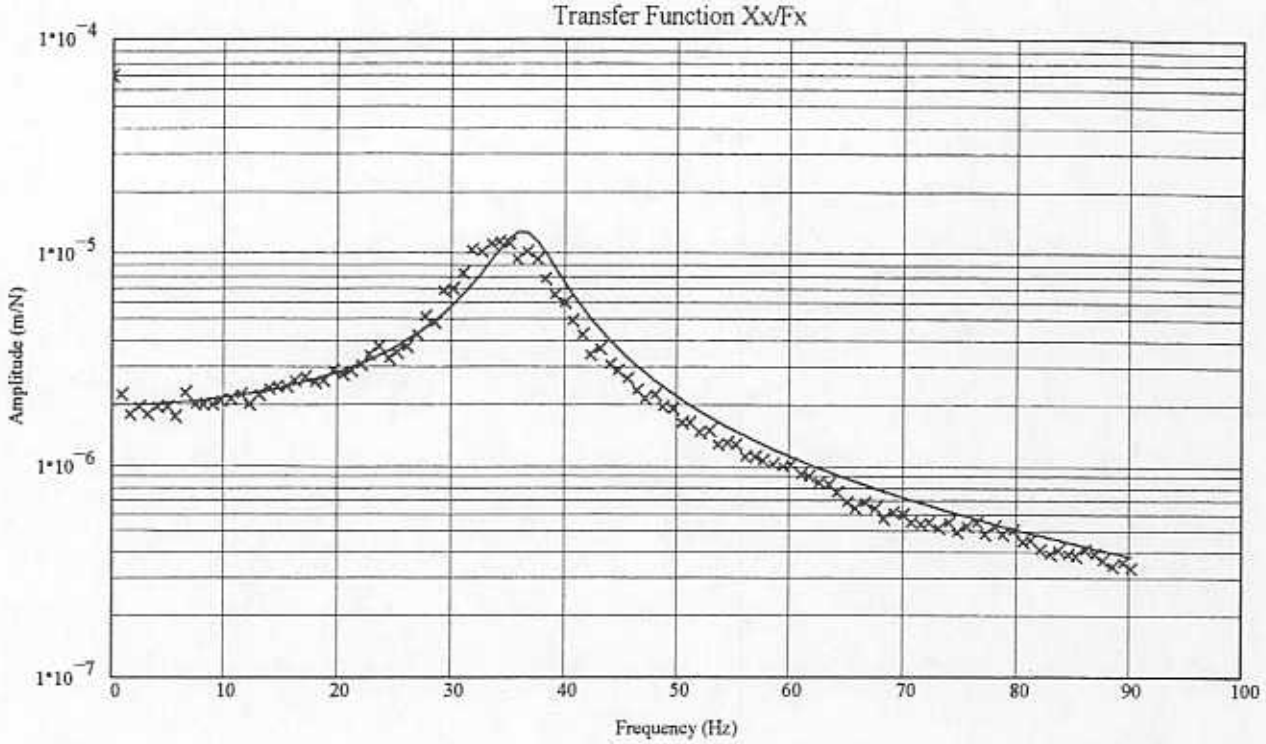

(a)

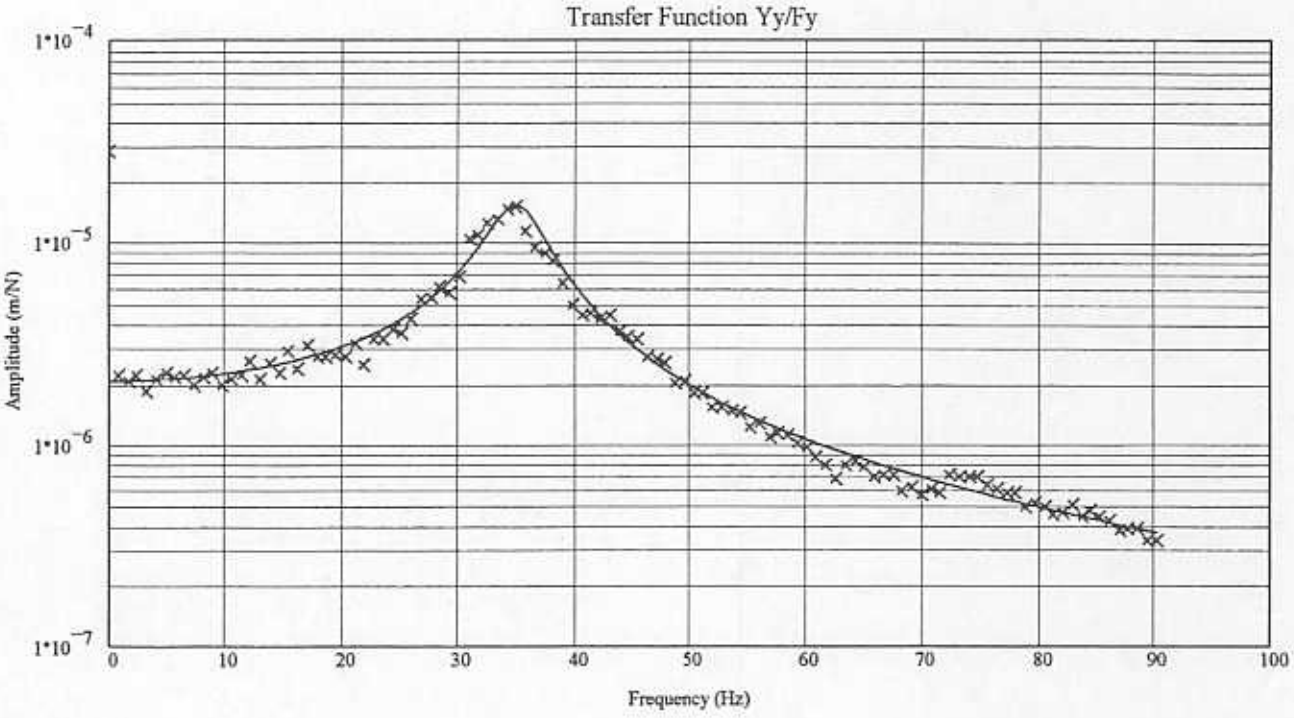

(b)

Figure 14 - Transfer functions for centered seal, no shaft rotation, pressure ratio = 1.50
symbols = tests, lines = curve fits)

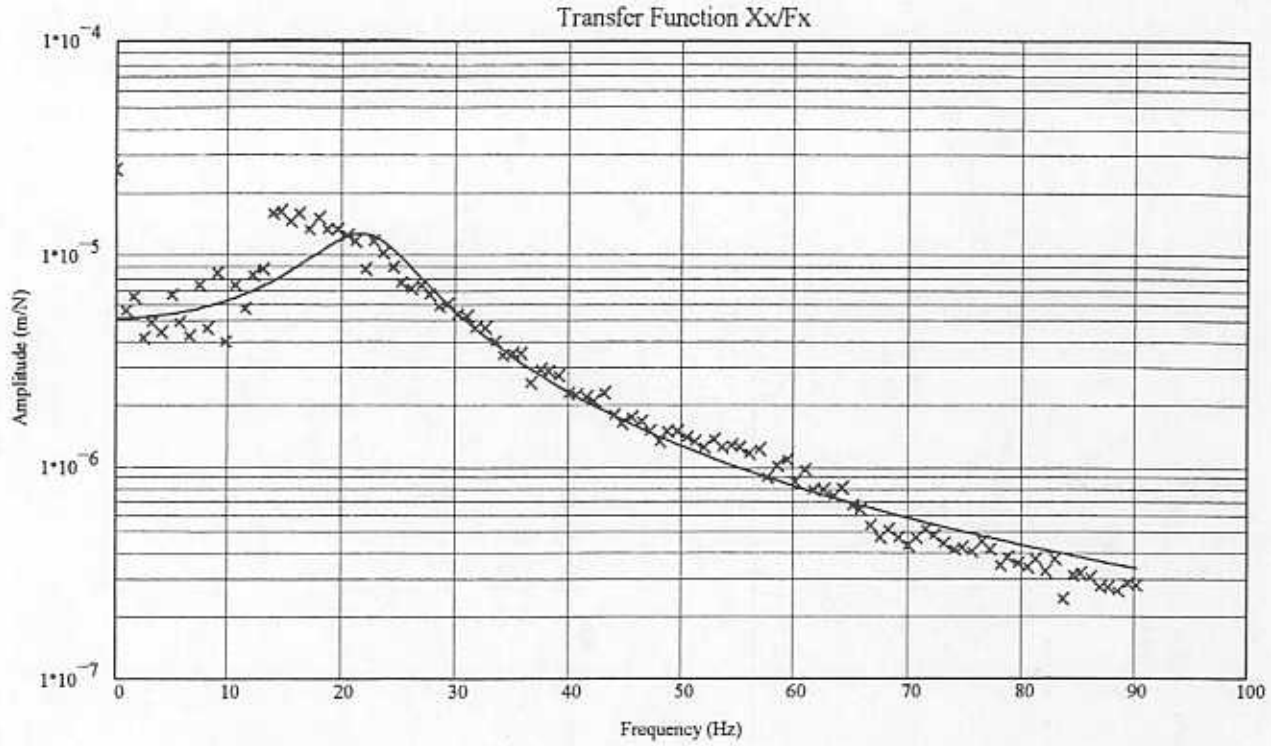

(a)

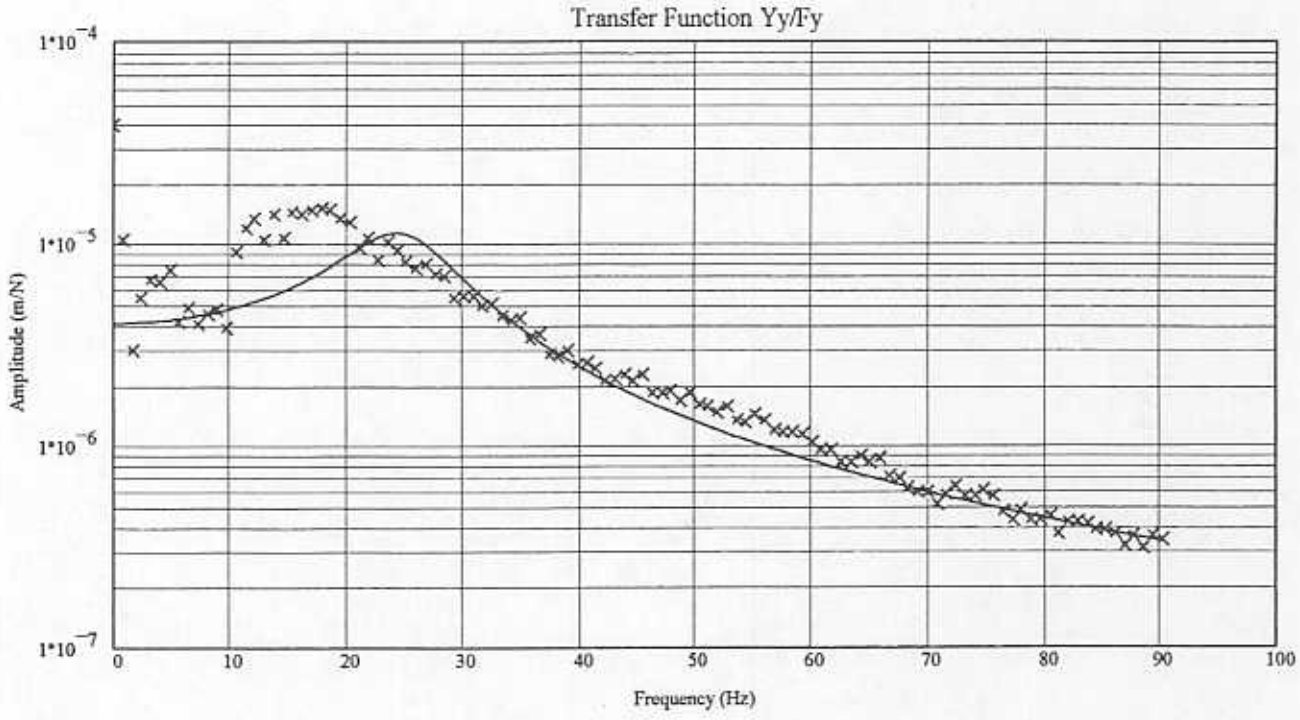

(b)

Figure 15 - Transfer functions for centered seal, no shaft rotation, pressure ratio = 1.75
(symbols = tests, lines = curve fits)

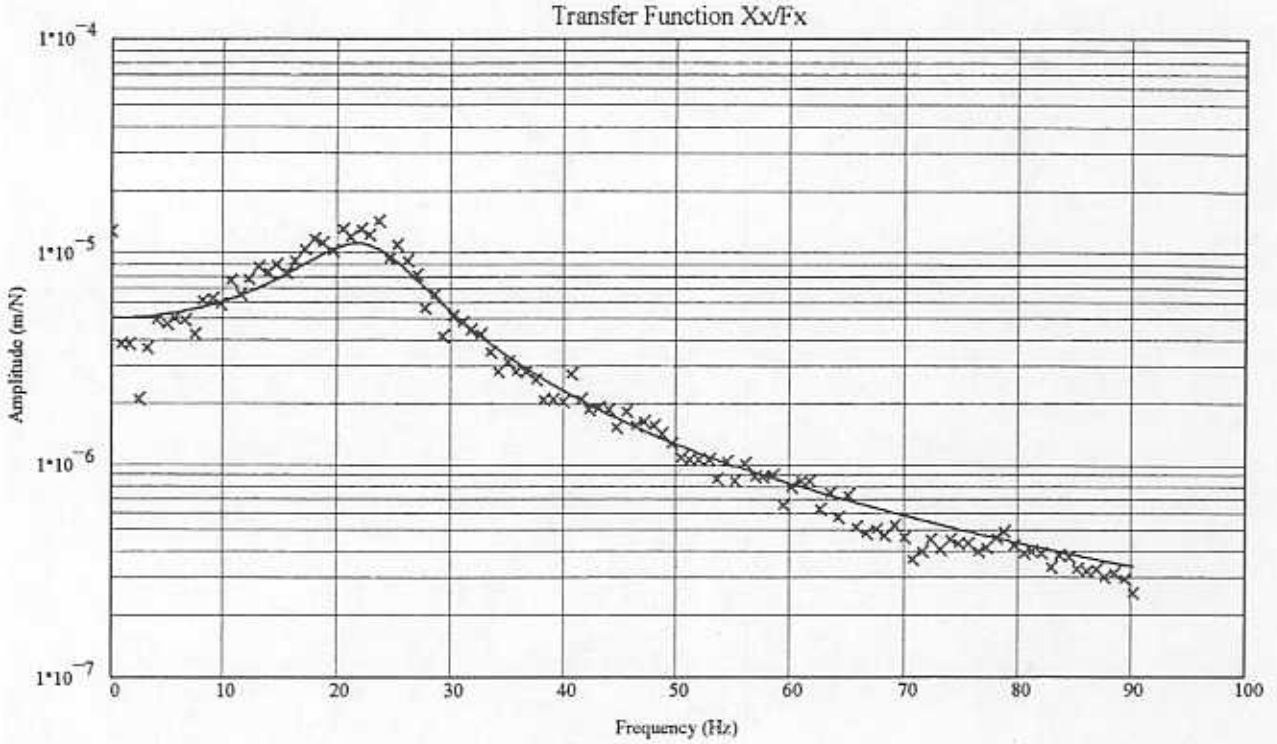

(a)

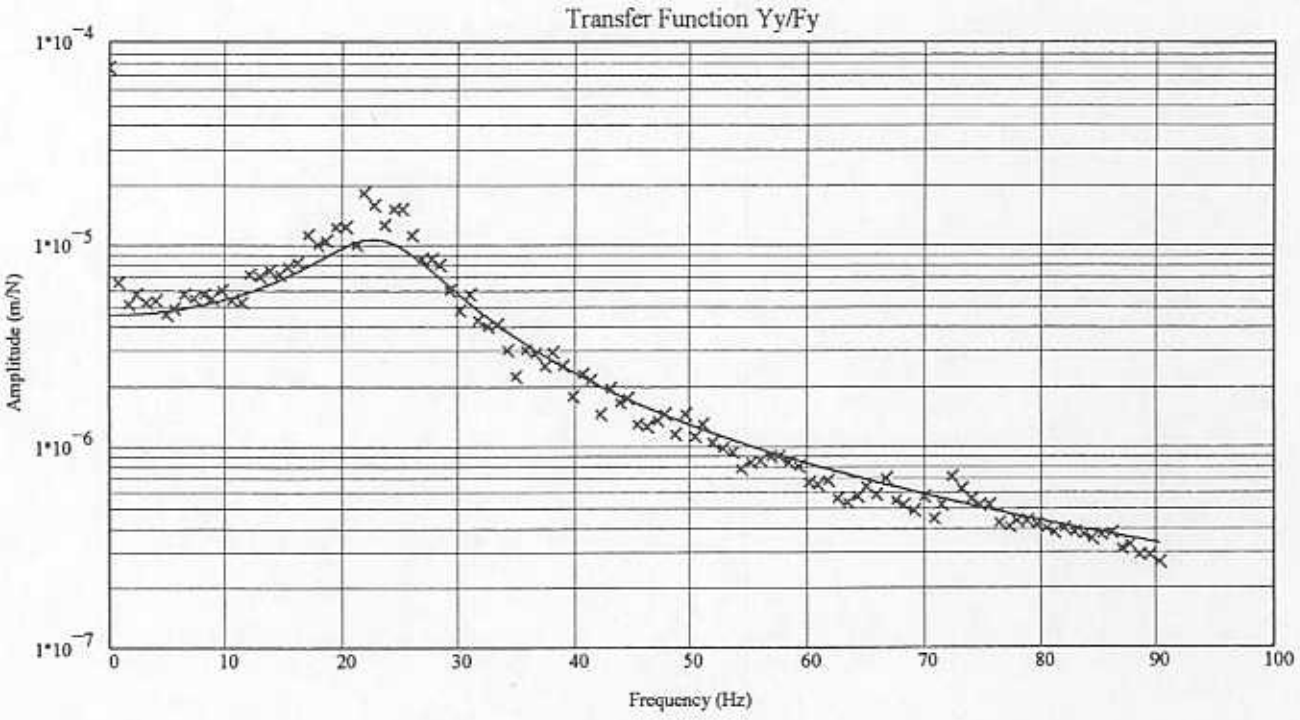

(b)

Figure 16 - Transfer functions for centered seal, no shaft rotation, pressure ratio = 2.00
(symbols = tests, lines = curve fits)

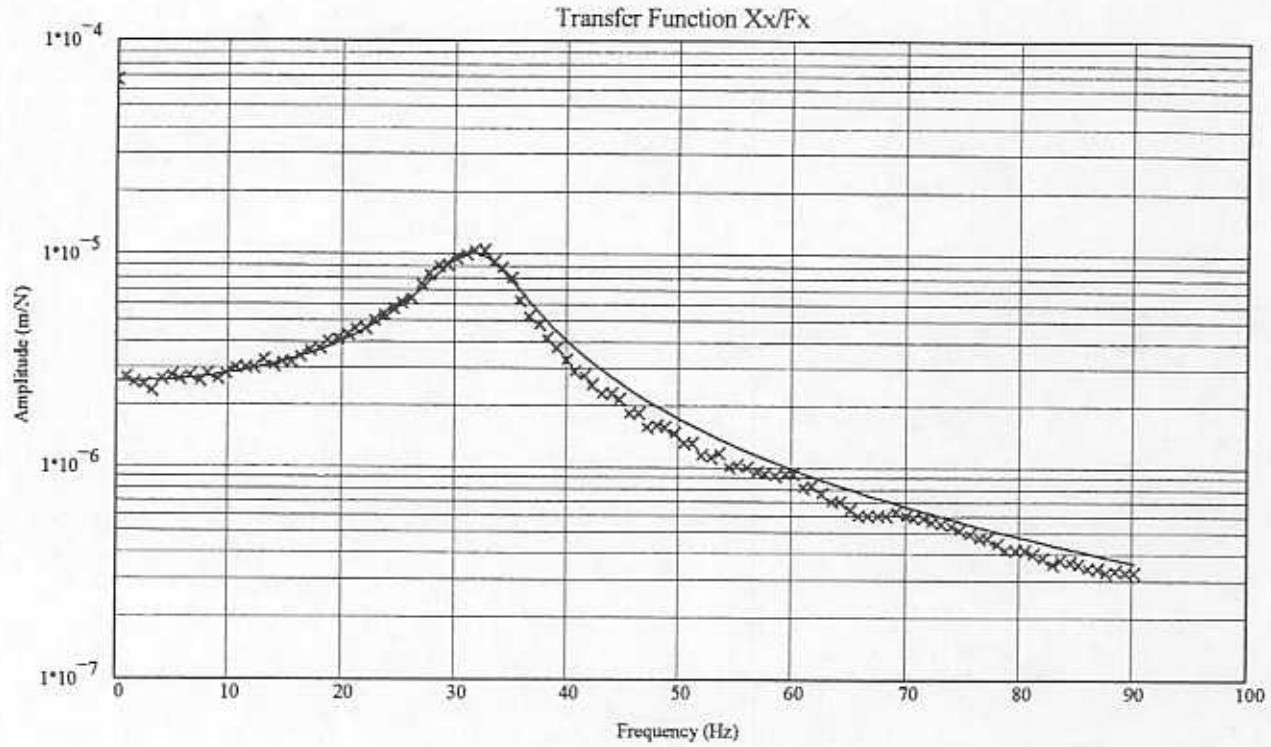

(a)

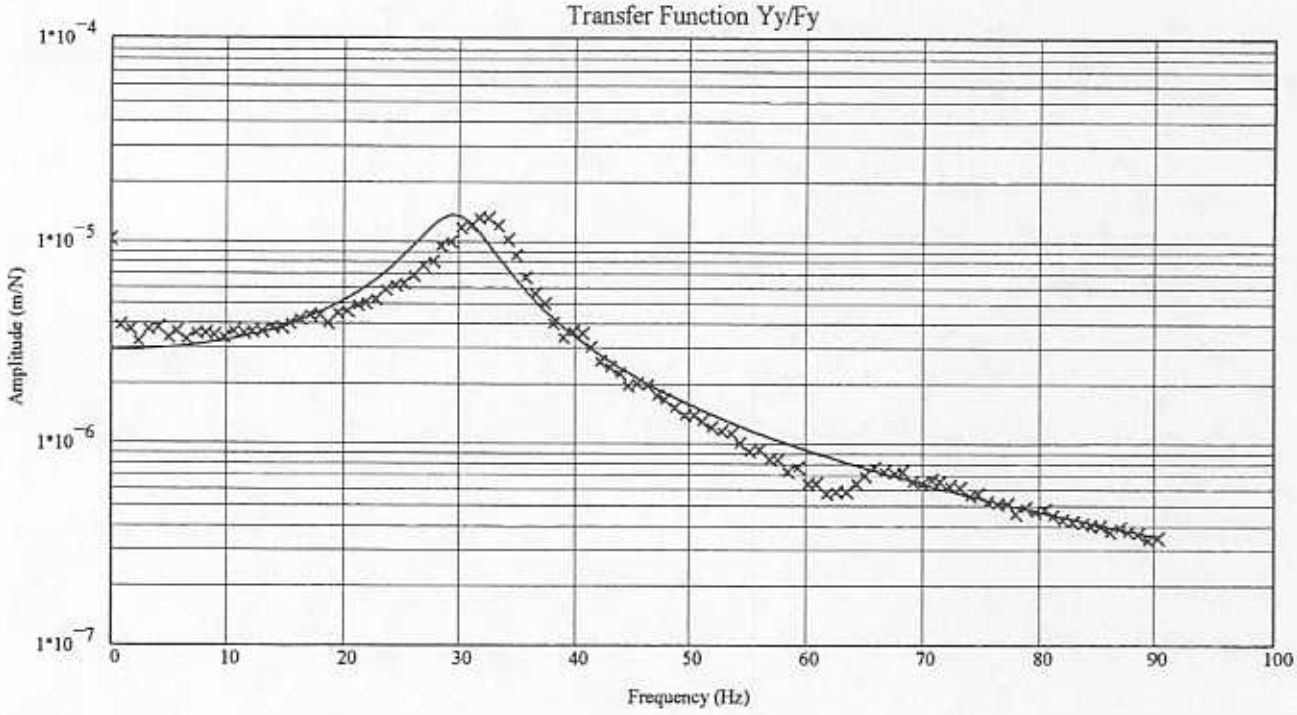

(b)

Figure 17 - Transfer functions for centered seal, no shaft rotation, pressure ratio = 2.25
(symbols = tests, lines = curve fits)

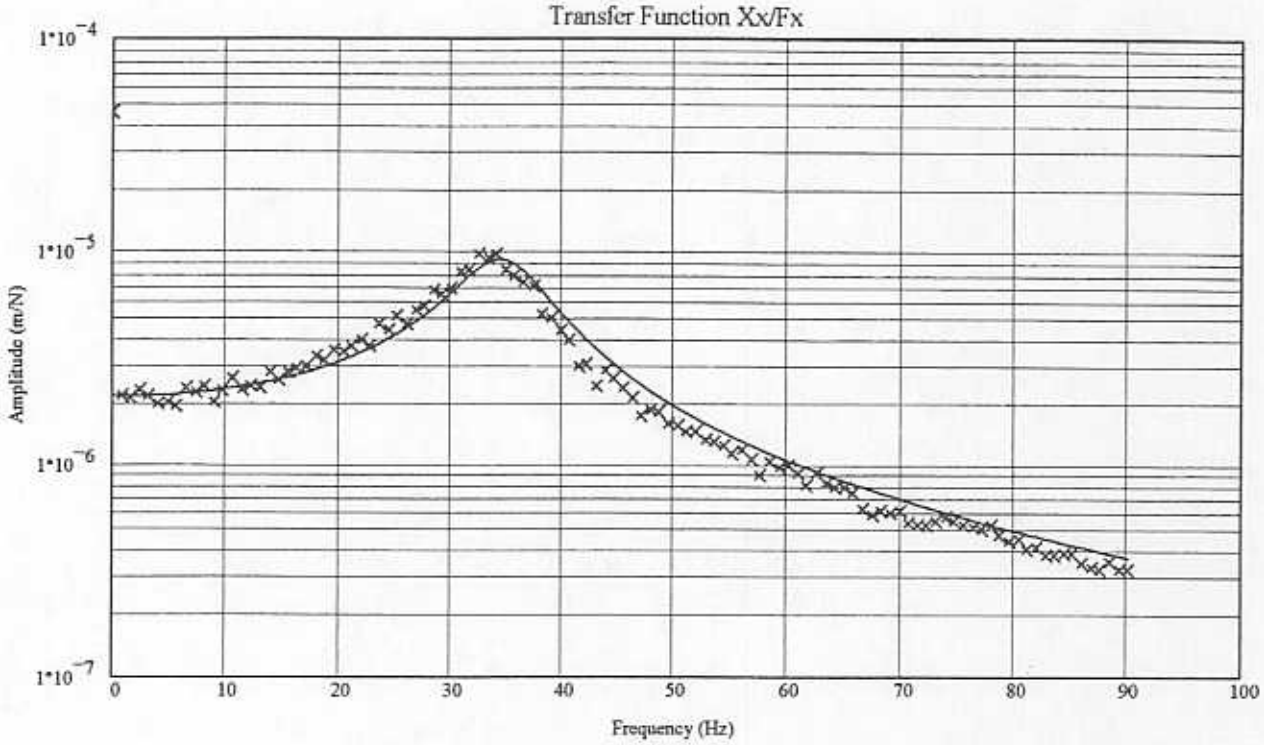

(a)

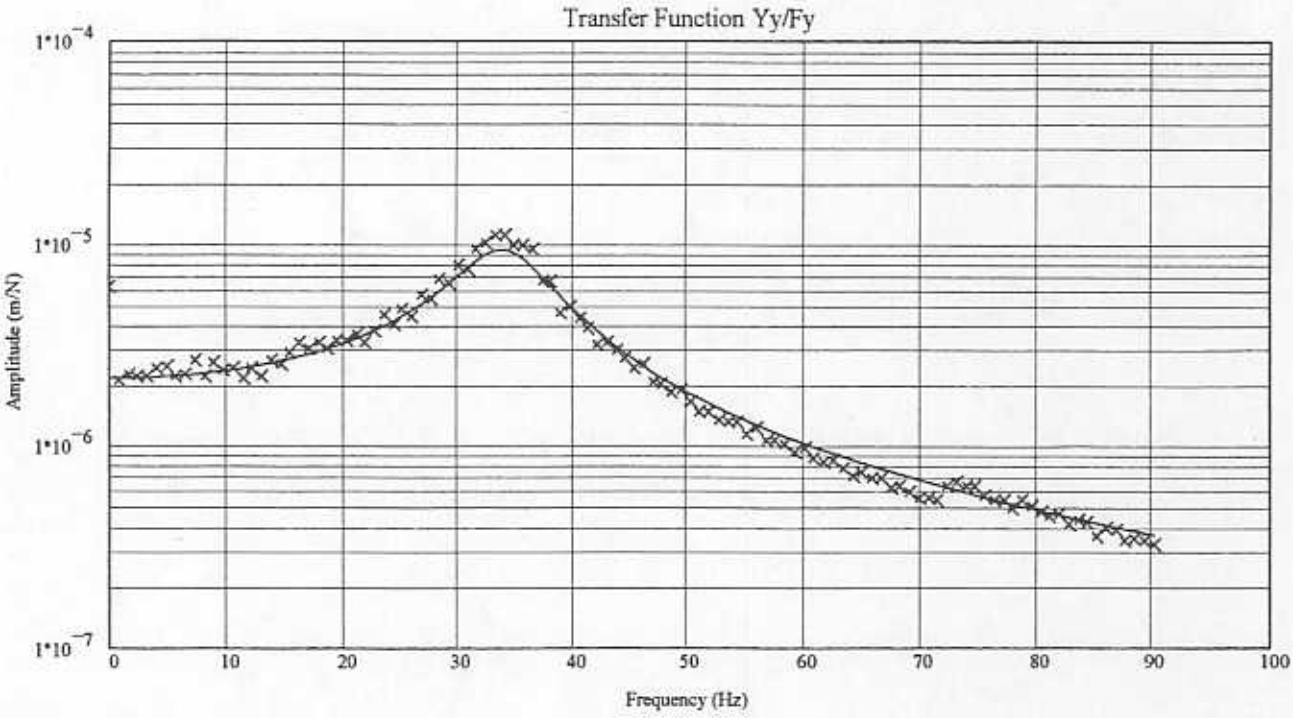

(b)

Figure 18 - Transfer functions for centered seal, no shaft rotation, pressure ratio = 2.50
(symbols = tests, lines = curve fits)

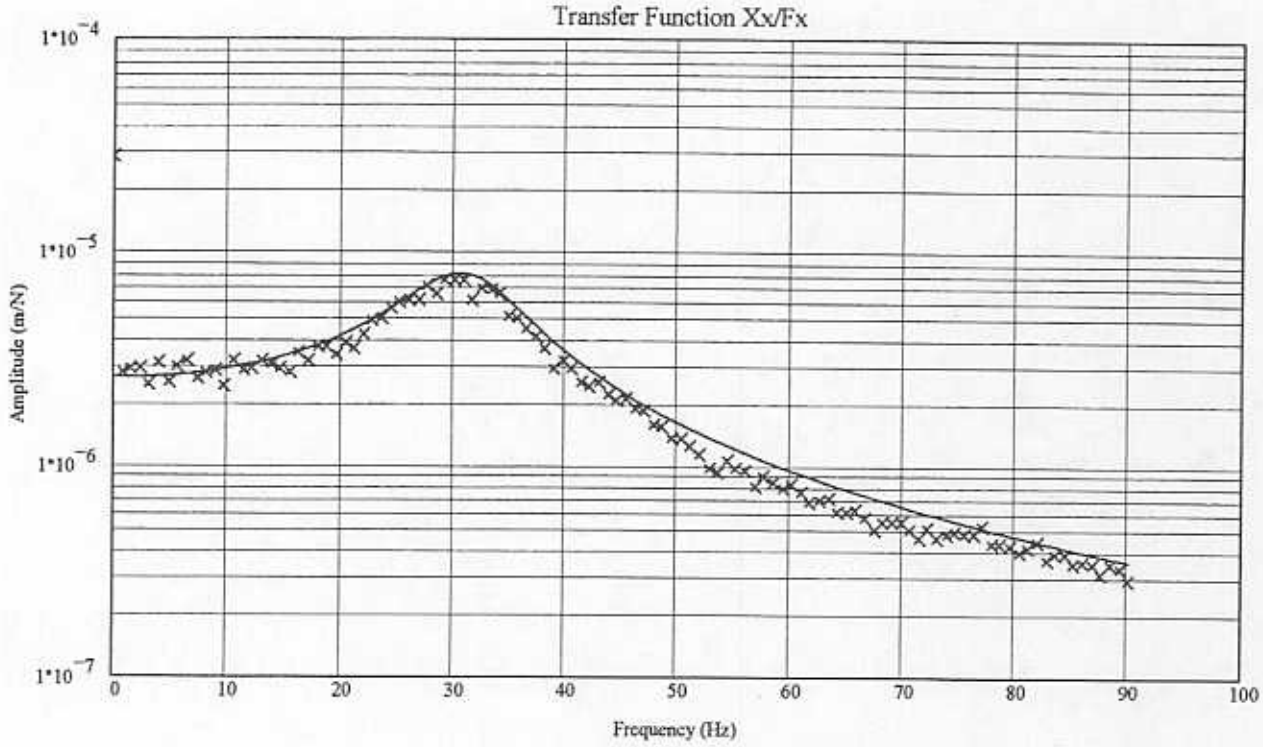

(a)

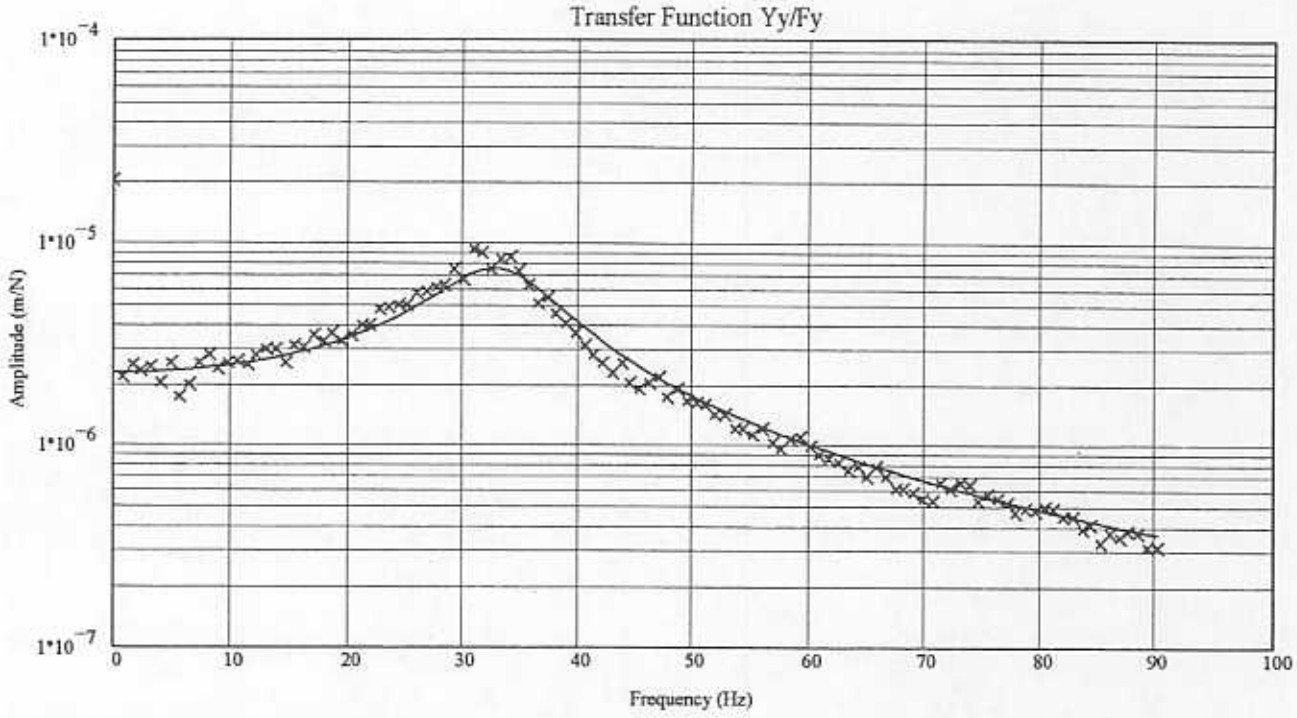

(b)

Figure 19 - Transfer functions for centered seal, no shaft rotation, pressure ratio = 3.00
(symbols = tests, lines = curve fits)

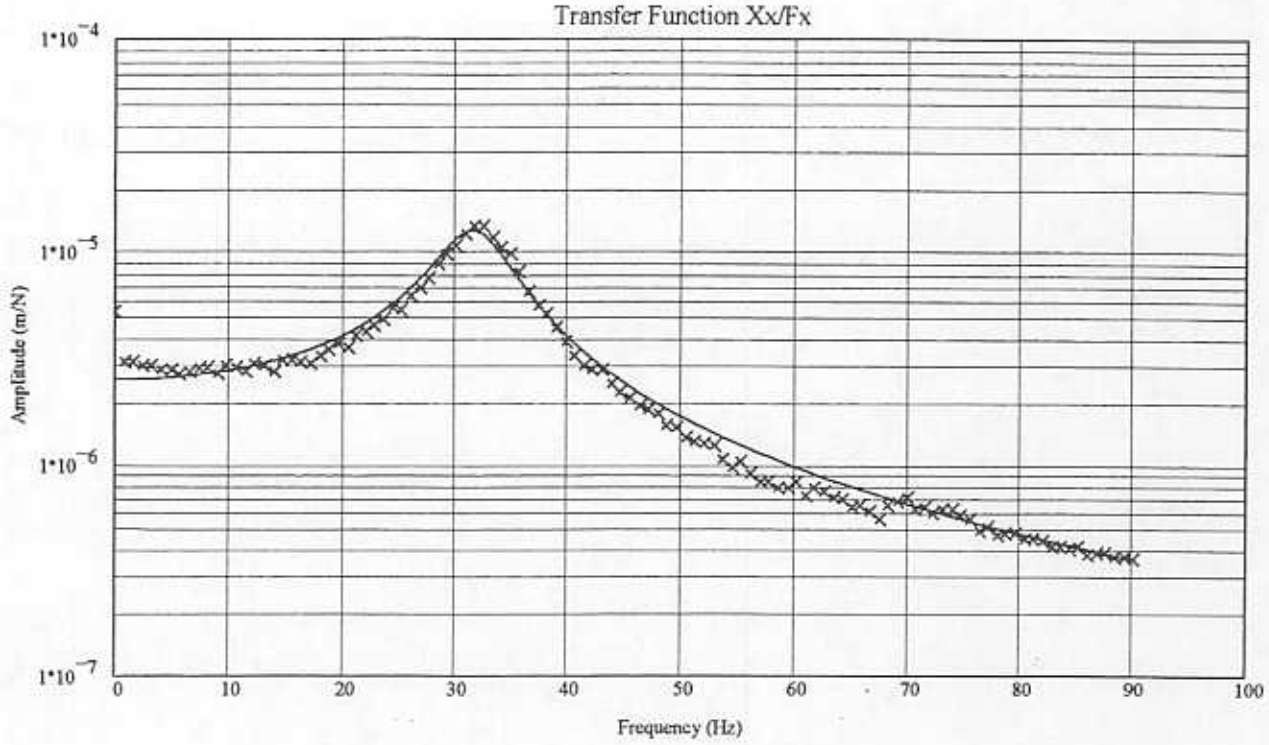

(a)

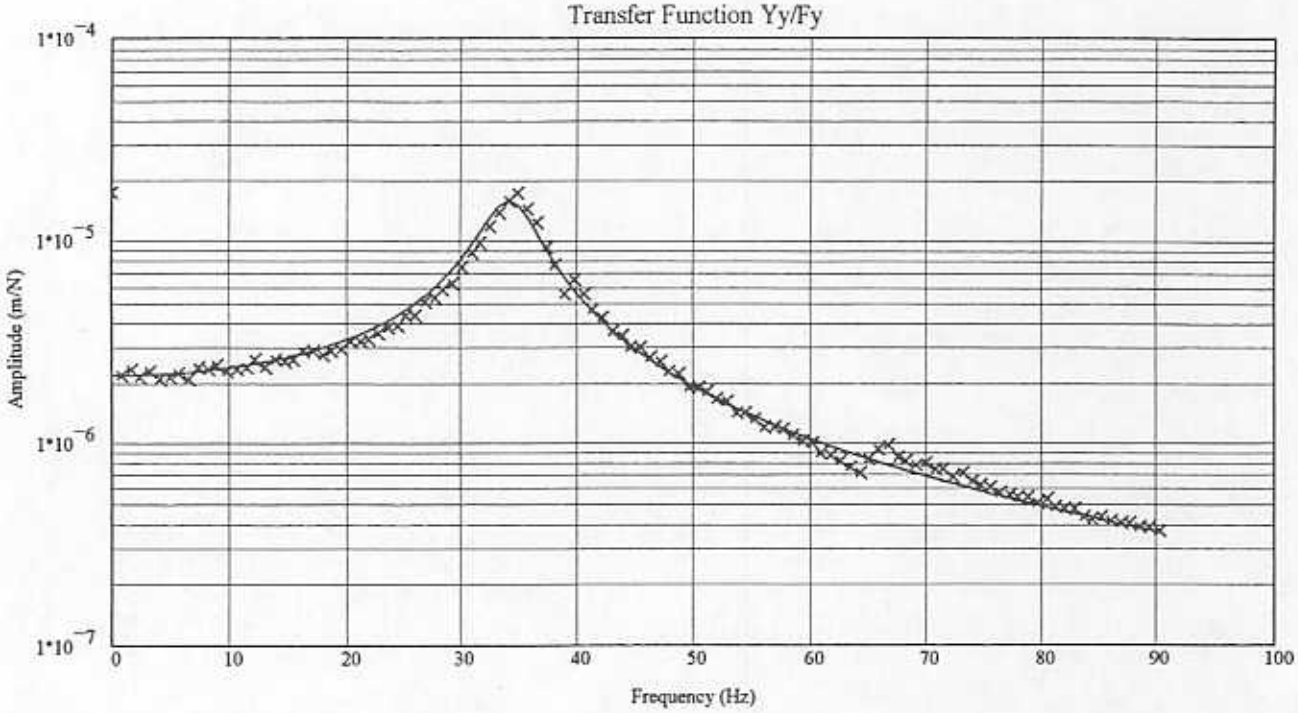

(b)

Figure 20 - Transfer functions for off-center seal, no shaft rotation, pressure ratio = 1.50
(symbols = tests, lines = curve fits)

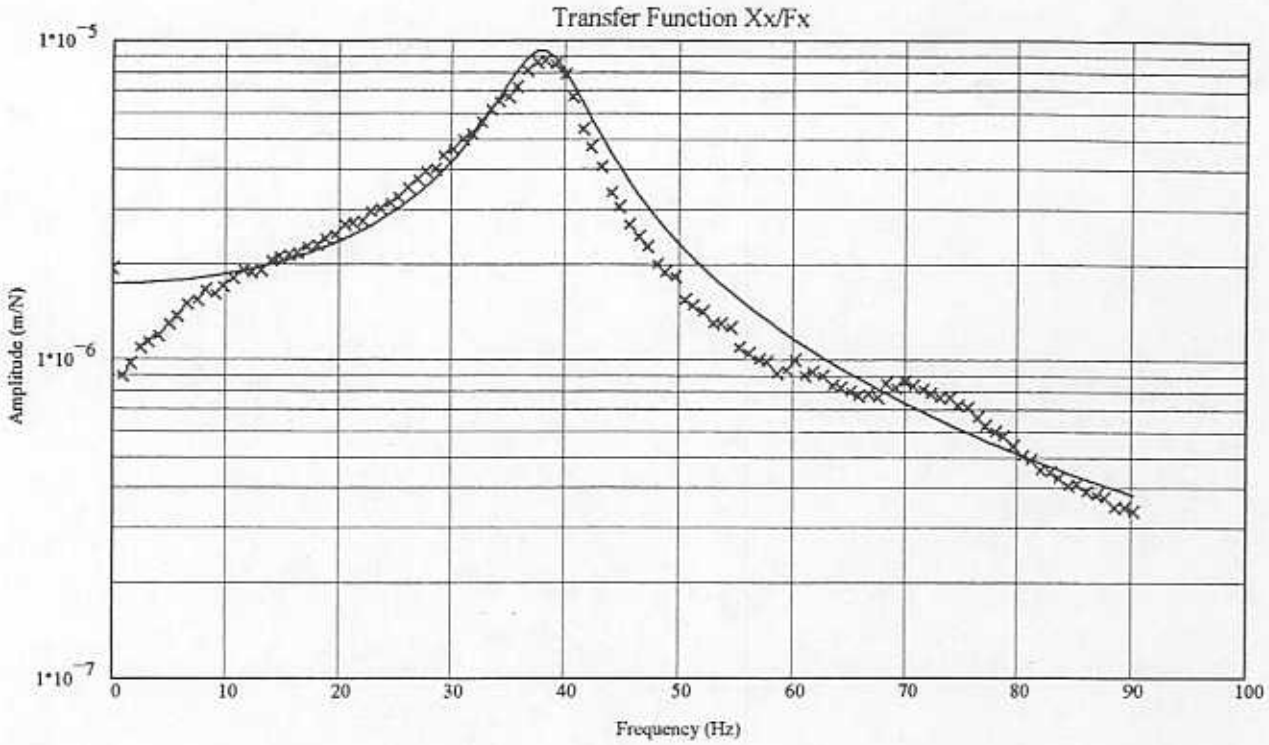

(a)

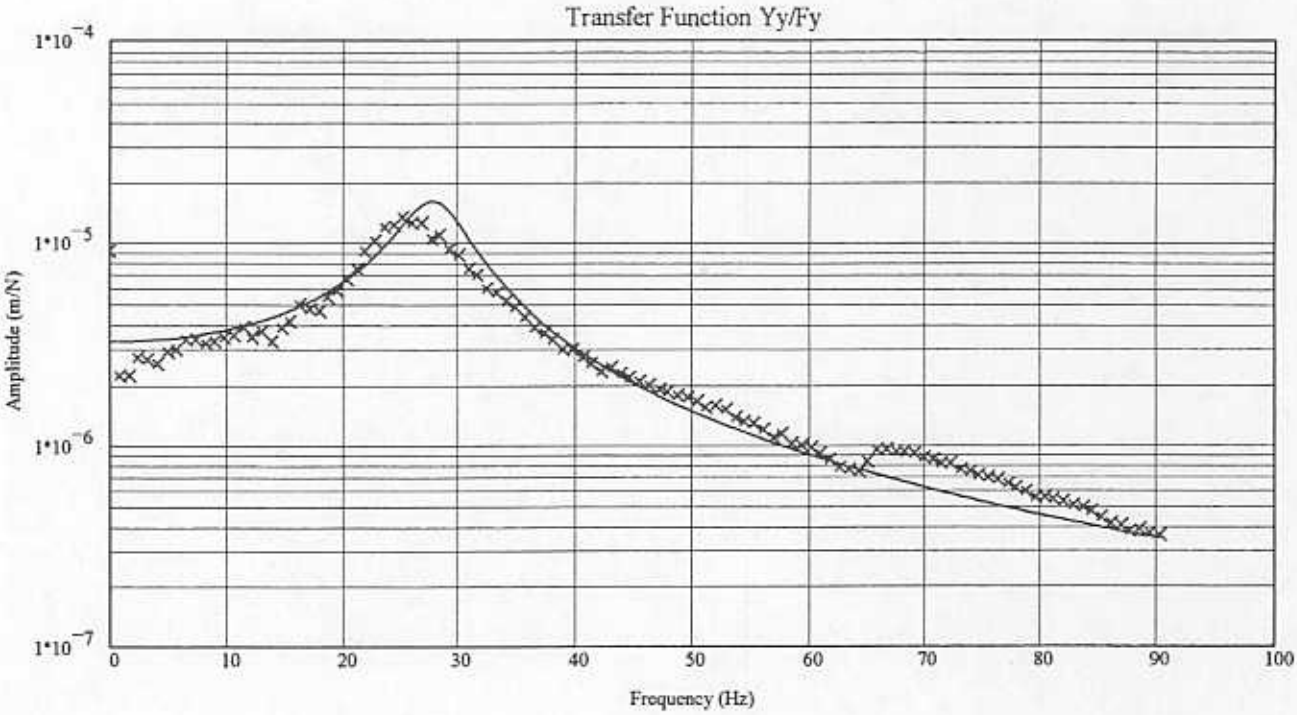

(b)

Figure 21 - Transfer functions for off-center seal, no shaft rotation, pressure ratio = 2.00
(symbols = tests, lines = curve fits)

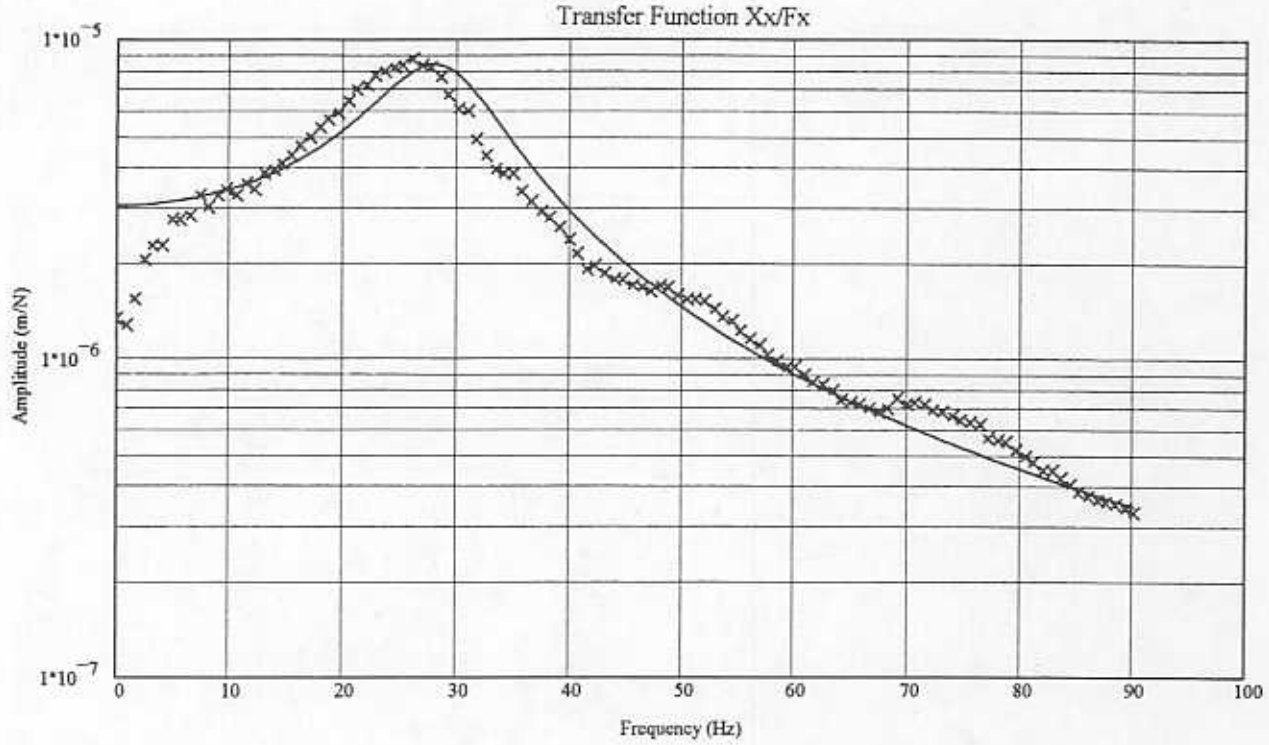

(a)

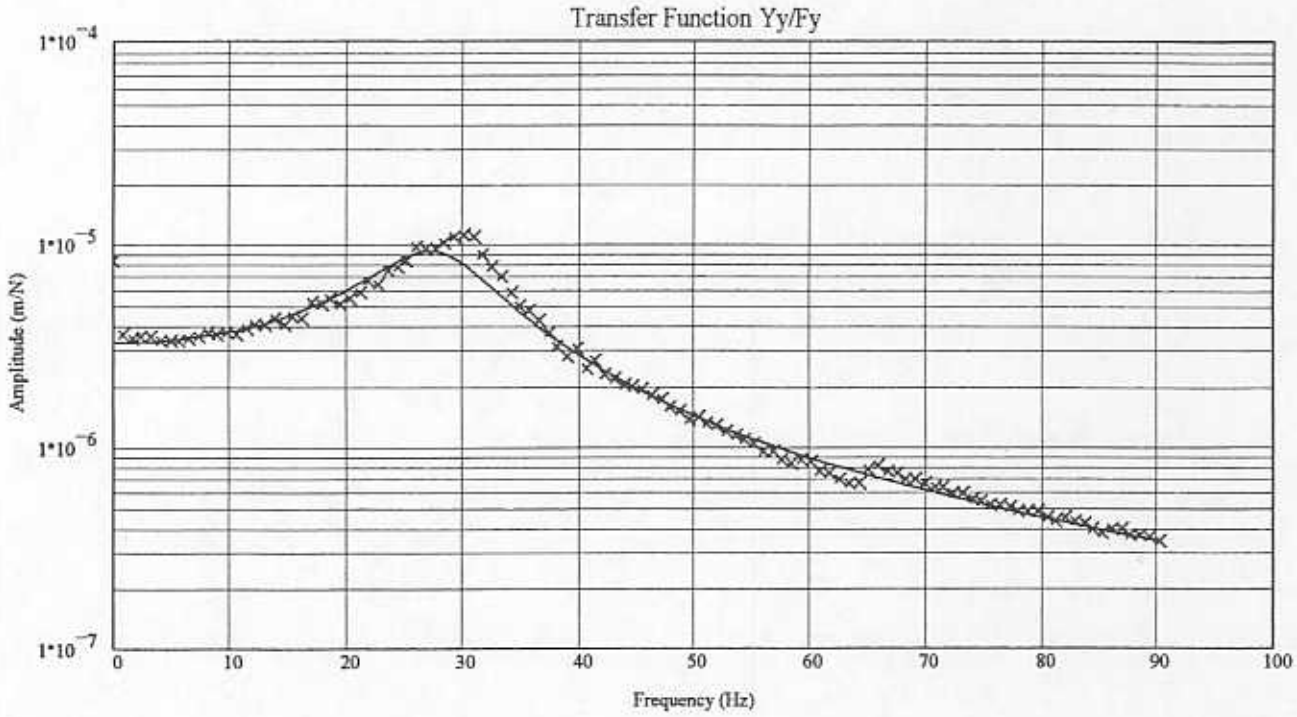

(b)

Figure 22 - Transfer functions for off-center seal, no shaft rotation, pressure ratio = 2.50
(symbols = tests, lines = curve fits)

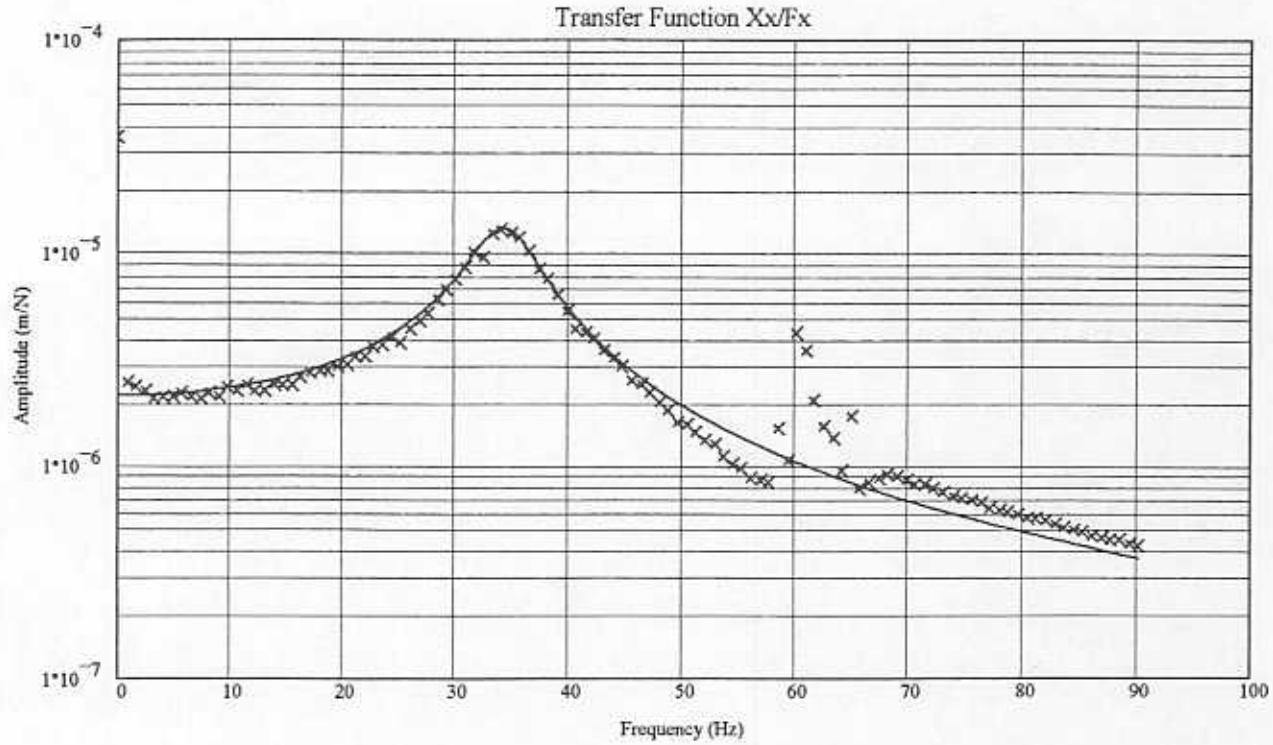

(a)

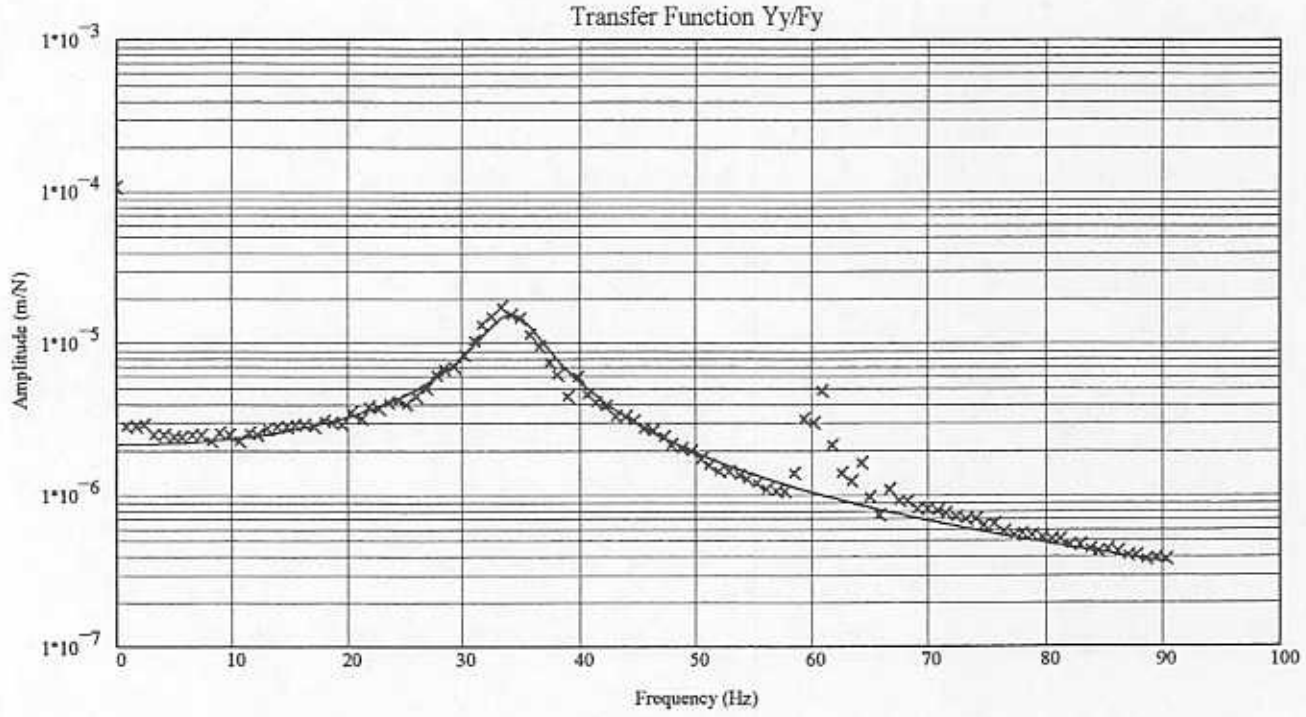

(b)

Figure 23 - Transfer functions for centered seal, shaft rotation = 3,600 rpm, pressure ratio = 1.50
(symbols = tests, lines = curve fits)

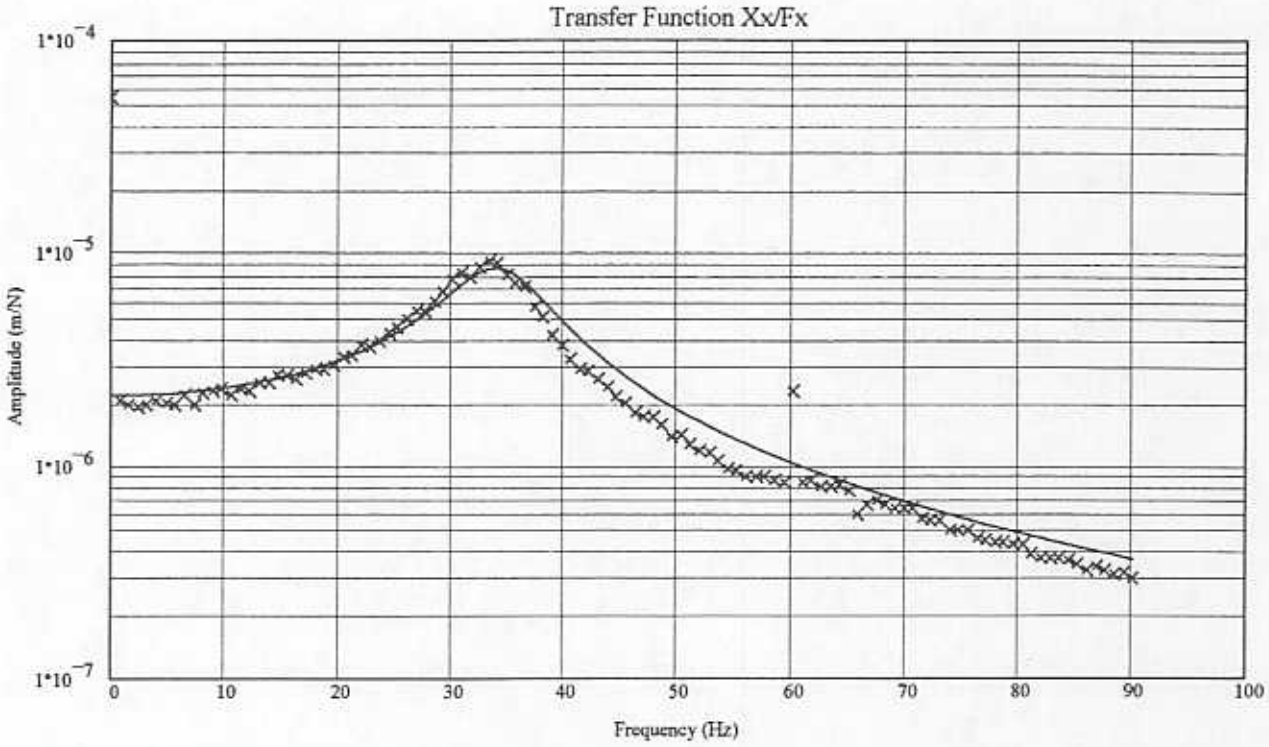

(a)

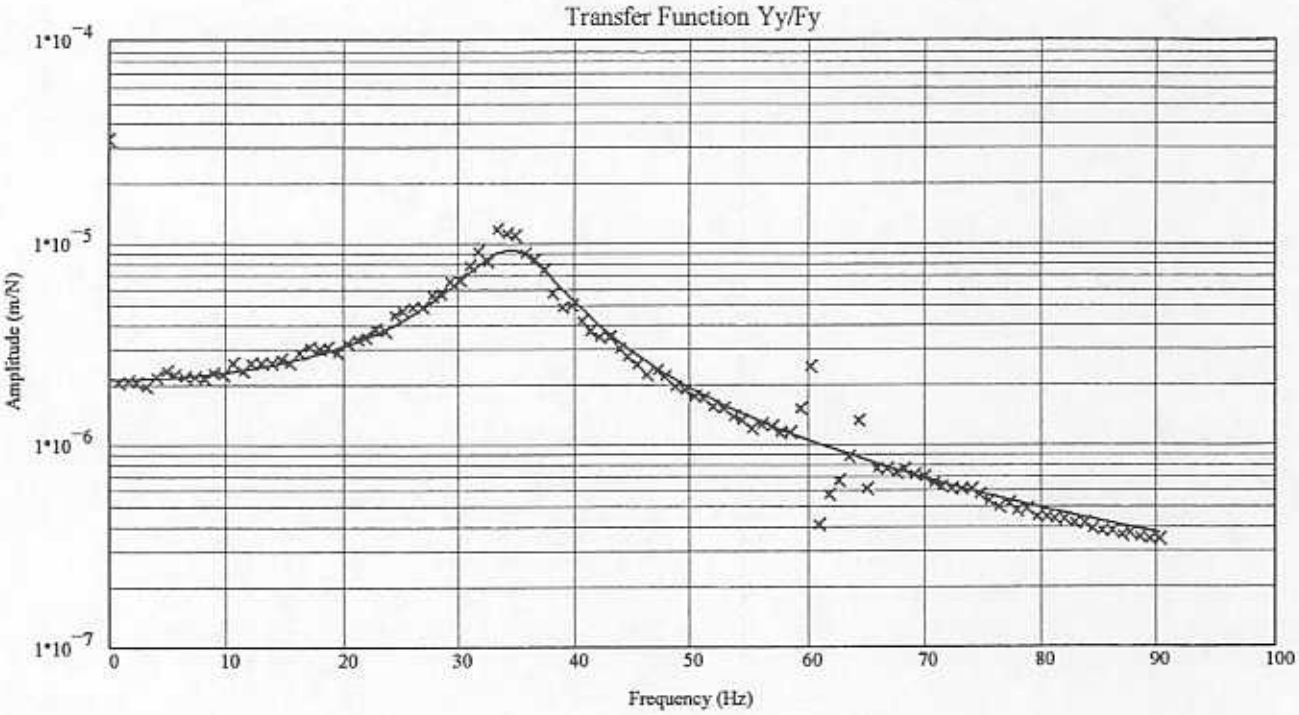

(b)

Figure 24 - Transfer functions for centered seal, shaft rotation = 3,600 rpm, pressure ratio = 2.00
(symbols = tests, lines = curve fits)

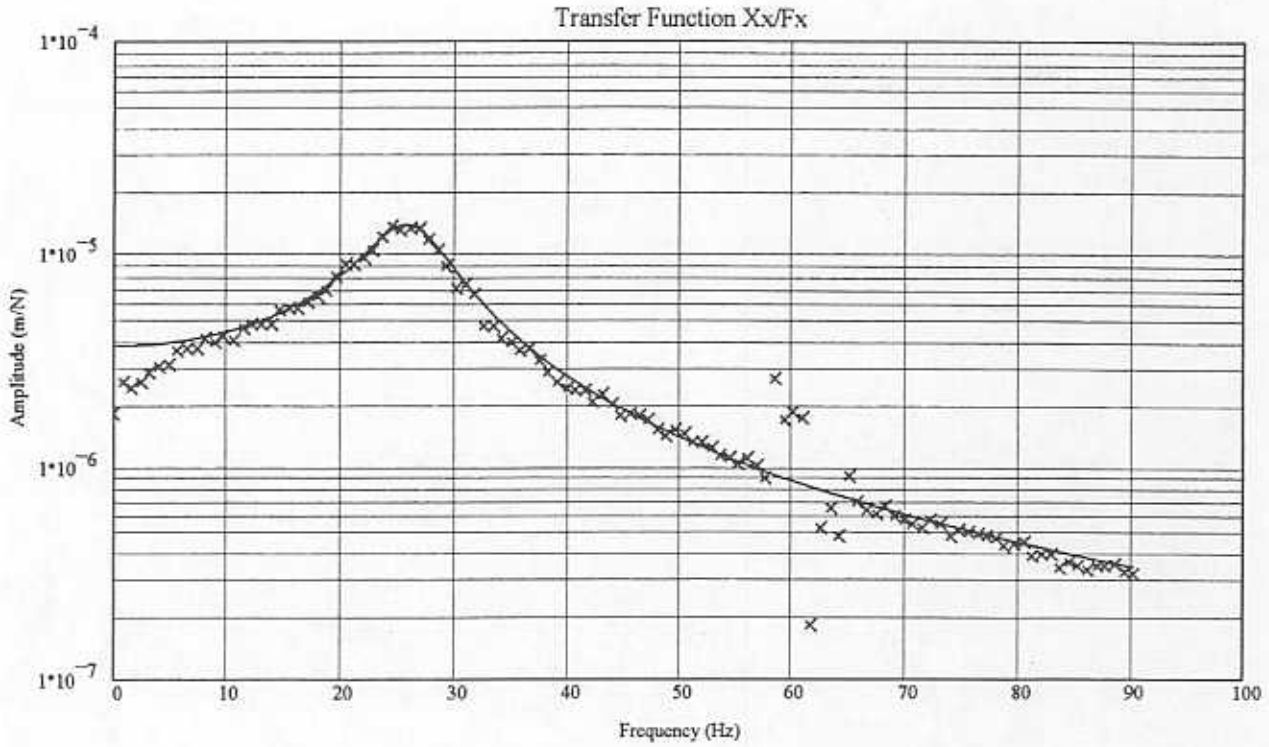

(a)

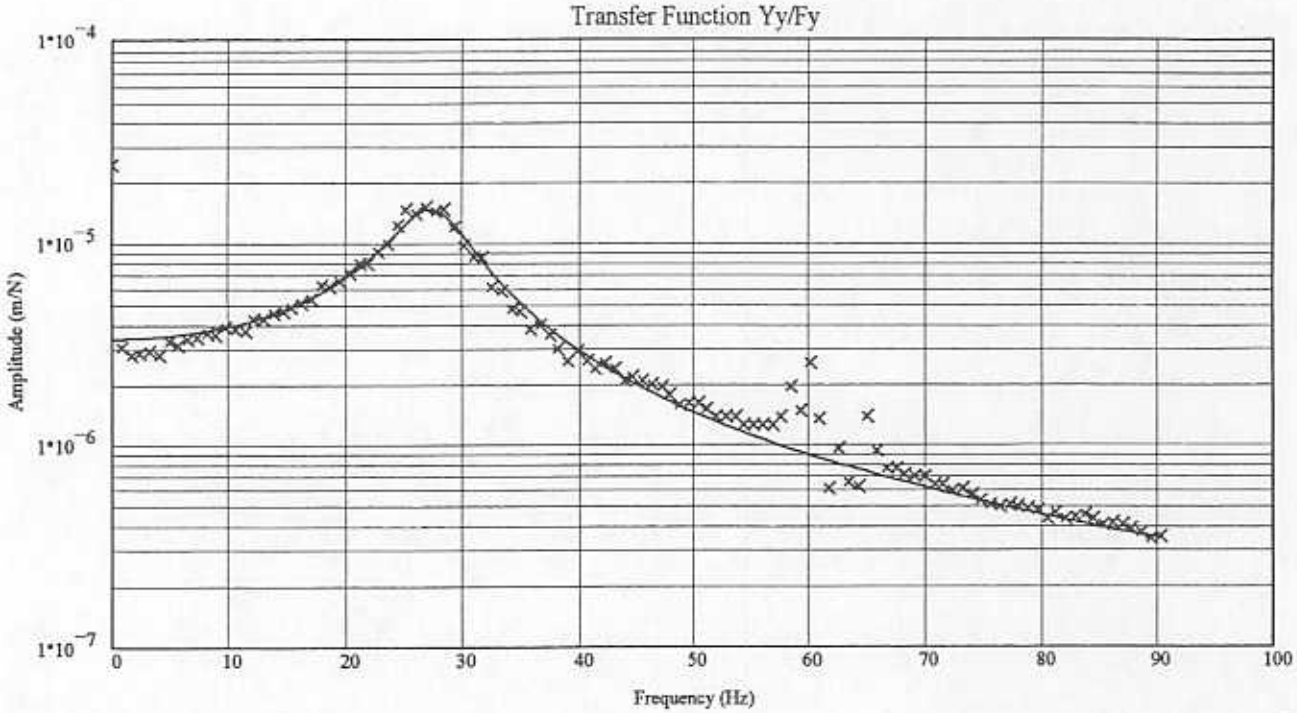

(b)

Figure 25 - Transfer functions for centered seal, shaft rotation = 3,600 rpm, pressure ratio = 2.50
(symbols = tests, lines = curve fits)

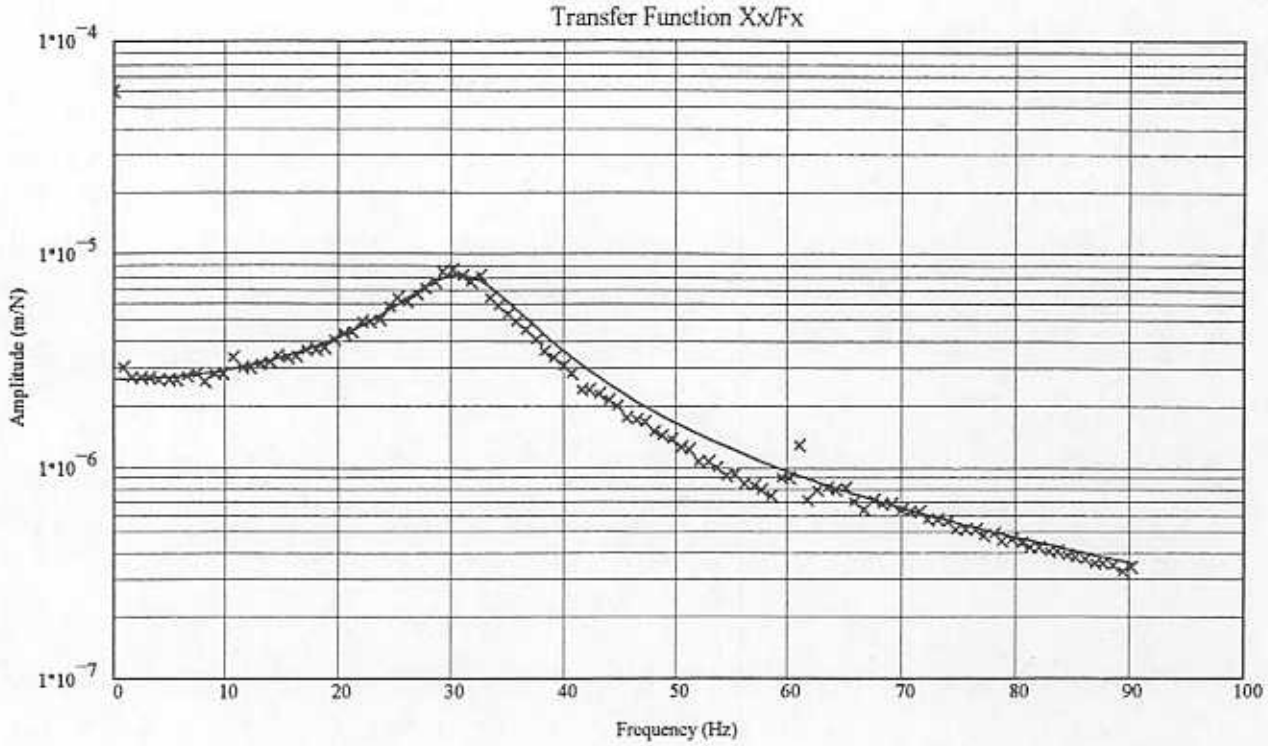

(a)

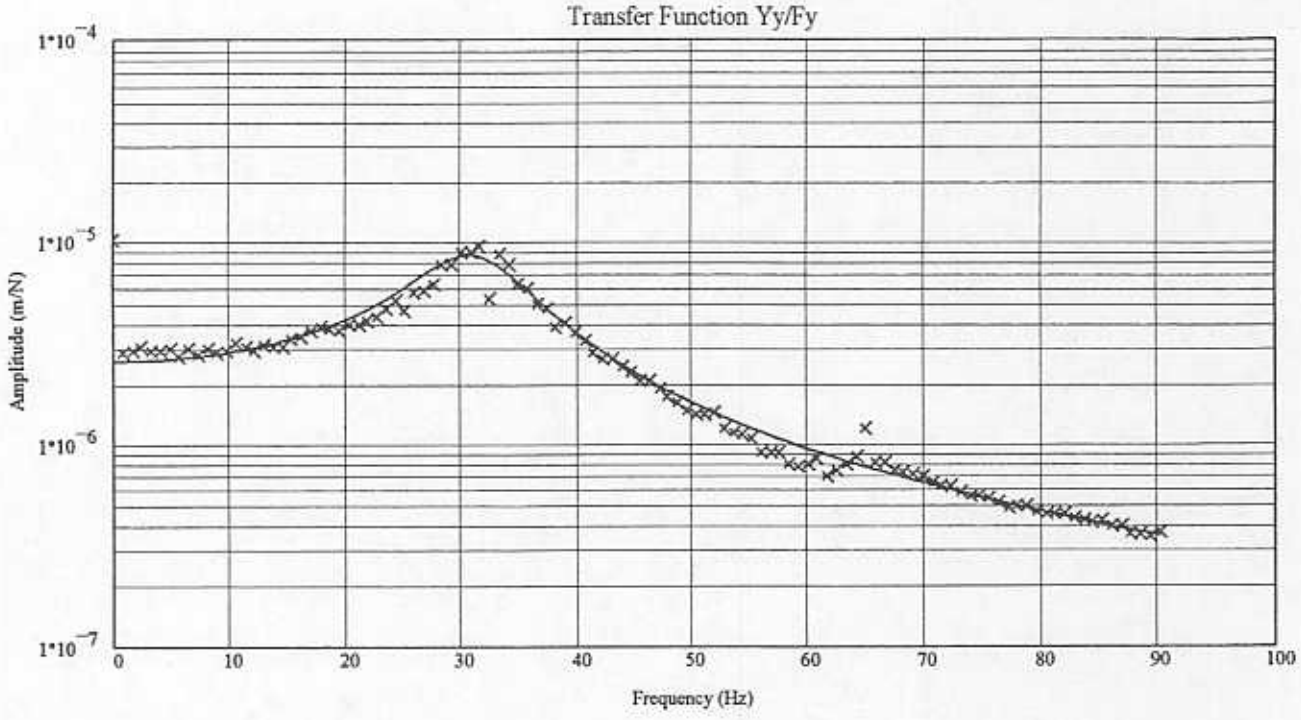

(b)

Figure 26 - Transfer functions for centered seal, shaft rotation = 3,600 rpm, pressure ratio = 3.00
(symbols = tests, lines = curve fits)

Table 8 - Estimated values and uncertainites for seal stiffness and damping coefficients

Speed (RPM)	Seal Static Position	Pressure Ratio	Kxx (kN/m)	Kyy (kN/m)	Cxx (N*sec/m)	Cyy (N*sec/m)
0	Centered	1.25	272	258	21	67
		1.50	242	233	191	187
		1.50	172	198	261	237
		1.75	-78	-2	416	462
		2.00	-73	-27	491	537
		2.00	2	-17	391	387
		2.25	127	98	341	287
		2.50	202	213	341	387
		2.50	192	188	391	337
		3.00	112	193	491	537
		3.00	117	183	491	537
0	Off-Center	1.50	122	213	241	187
		2.00	297	58	291	247
		2.50	52	58	511	517
3600	Centered	1.50	192	213	191	187
		1.50	222	223	191	187
		2.00	-8	48	291	287
		2.00	-53	-2	341	387
		2.50	192	228	391	387
		2.50	172	188	391	397
		3.00	112	138	491	487
		3.00	162	158	441	437

Uncertainties

Speed (RPM)	Seal Static Position	Pressure Ratio	U(Kxx) (kN/m)	U(Kyy) (kN/m)	U(Cxx) (N*sec/m)	U(Cyy) (N*sec/m)
0	Centered	1.25	6	6	6	6
		1.50	6	6	8	8
		1.50	6	6	12	12
		1.75	2	2	17	17
		2.00	2	2	20	20
		2.00	2	2	15	15
		2.25	3	3	14	14
		2.50	4	4	14	14
		2.50	4	4	15	15
		3.00	2	2	20	20
		3.00	2	2	20	20
0	Off-Center	1.50	2	4	12	8
		2.00	6	2	12	12
		2.50	2	2	20	20
3600	Centered	1.50	4	4	8	8
		1.50	4	4	8	8
		2.00	2	2	12	12
		2.00	2	2	15	15
		2.50	4	4	15	15
		2.50	4	4	15	15
		3.00	2	2	20	20
		3.00	4	4	17	17

Table 9 - Measured values and uncertainty for temperature, pressure and mass flow rate

Speed (RPM)	Seal Static Position	Pressure Ratio	T_1 (F)	T_2 (F)	P_1 (PSIG)	P_2 (PSIG)	P_3 (PSIG)	$\dot{m}$ (kg/sec)	
0	Centered	1.25	71	n/a	3.7	91	88	0.0070	
		1.50	74	n/a	7.4	79	76	0.0098	*
		1.50	72	n/a	7.4	78	75	0.0129	
		1.75	72	n/a	11.0	78	74	0.0155	
		2.00	75	n/a	14.7	75	70	0.0145	*
		2.00	73	n/a	14.7	70	64	0.0204	
		2.25	74	n/a	18.4	95	90	0.0181	
		2.50	74	n/a	22.0	74	69	0.0241	*
		2.50	74	n/a	22.0	95	88	0.0206	
		3.00	75	n/a	29.4	68	61	0.0262	*
		3.00	74	n/a	29.4	82	76	0.0272	
0	Off-Center	1.50	70	n/a	7.4	95	90	0.0108	
		2.00	70	n/a	14.7	95	88	0.0164	
		2.50	71	n/a	22.0	90	87	0.0206	
3600	Centered	1.50	71	110	7.4	95	90	0.0108	
		1.50	72	114	7.4	95	90	0.0111	
		2.00	72	113	14.7	95	90	0.0159	
		2.00	74	117	14.7	95	89	0.0164	
		2.50	72	116	22.0	95	90	0.0205	
		2.50	74	115	22.0	90	82	0.0215	
		3.00	72	115	29.4	90	80	0.0262	
		3.00	75	118	29.4	80	70	0.0285	

Uncertainties

Speed (RPM)	Seal Static Position	Pressure Ratio	$U(T_1)$ (F)	$U(T_2)$ (F)	$U(P_1)$ (PSIG)	$U(P_2)$ (PSIG)	$U(P_3)$ (PSIG)	$U(\dot{m})$ (kg/sec)	
0	Centered	1.25	1	n/a	0.2	2	2	0.0006	
		1.50	1	n/a	0.2	2	2	0.0013	*
		1.50	1	n/a	0.2	2	2	0.0010	
		1.75	1	n/a	0.2	2	2	0.0012	
		2.00	1	n/a	0.2	2	2	0.0019	*
		2.00	1	n/a	0.2	2	2	0.0016	
		2.25	1	n/a	0.2	2	2	0.0014	
		2.50	1	n/a	0.2	2	2	0.0031	*
		2.50	1	n/a	0.2	2	2	0.0016	
		3.00	1	n/a	0.2	2	2	0.0034	*
		3.00	1	n/a	0.2	2	2	0.0022	
0	Off-Center	1.50	1	n/a	0.2	2	2	0.0108	
		2.00	1	n/a	0.2	2	2	0.0164	
		2.50	1	n/a	0.2	2	2	0.0206	
3600	Centered	1.50	1	1	0.2	2	2	0.0108	
		1.50	1	1	0.2	2	2	0.0111	
		2.00	1	1	0.2	2	2	0.0159	
		2.00	1	1	0.2	2	2	0.0164	
		2.50	1	1	0.2	2	2	0.0205	
		2.50	1	1	0.2	2	2	0.0215	
		3.00	1	1	0.2	2	2	0.0262	
		3.00	1	1	0.2	2	2	0.0285	

* measured with visual type flow meter

APPENDIX A. Estimation of parameters' uncertainty on the frequency domain

The following MathCad analysis transforms the measurement uncertainties from the time domain to the frequency domain. First, the time domain increment and the number of data points is defined.

Time step

$dt := 0.00015$ sec

Number of samples

$tmax := 8192$

Counter for time step

$t := 0, 1 .. tmax - 1$

Frequency domain increment (inverse of the total sampling time) (Hz)

$$\Delta f := \frac{1}{dt \cdot tmax}$$

$\Delta f = 0.814$ Hz

Define the measurement uncertainties in the time domain

Force

$delf := 0.8$ N

Displacement

$delx := 0.000002$ m

Frequency

$delw := \Delta f \cdot 2 \cdot \pi$ rad/sec

To generate the time domain impulse, the impact must be defined as a magnitude and duration. In this case, the impact will last one time step, dt.

Impact magnitude

$af1 := 800$ N

Impact duration

$\Delta t1 := dt$ sec

To generate the time domain displacement response, the seal stiffness, damping and mass must be defined

Stiffness

$K1 := 400000$ N/m

Damping

$C1 := 500$ N sec/m

Mass

$M1 := 10$ Kg

The following calculations are necessary for the calculation of the free response to the impulse load

Natural frequency

$$\omega 1 := \sqrt{\frac{K1}{M1}}$$

$\omega 1 = 200$ rad/sec

Initial velocity

$$v_{01} := \frac{af1 \cdot \Delta t1}{M1}$$

$v_{01} = 0.012$ m/sec

Damping ratio

$$\xi 1 := \frac{C1}{2 \cdot \omega 1 \cdot M1}$$

$\xi 1 = 0.125$

Damped natural frequency

$$\omega_{d1} := \omega 1 \cdot \sqrt{1 - \xi 1^2}$$

$$\omega_{d1} = 198.431 \quad \text{rad/sec}$$

The time domain impulse is generated using the Dirac delta function so that the force is maximum when t=0, and zero for the remaining time. Two forcing functions are created, one which is one magnitude of uncertainty less than the original force, and one that is one magnitude greater than the original force.

$$f1_t := \delta(0,t) \cdot (af1 - delf)$$

$$f2_t := \delta(0,t) \cdot (af1 + delf)$$

The displacement response is the exact solution for the free response of a single-degree-of-freedom system to an initial velocity. The initial velocity is a function of the impulse. Two displacement functions are created. One which which responds with one order of magnitude larger displacement than original and responds at a frequency one order of magnitude larger than the original response frequency. The second response is just the opposite.

$$x1_t := e^{-\xi 1 \cdot (\omega 1 + delw) \cdot t \cdot dt} \cdot \left[\left(\frac{v_{01}}{\omega_{d1}} + delx \right) \cdot \sin\left[\left(\omega_{d1} + delw \right) \cdot t \cdot dt \right] \right]$$

$$x2_t := e^{-\xi 1 \cdot (\omega 1 - delw) \cdot t \cdot dt} \cdot \left[\left(\frac{v_{01}}{\omega_{d1}} - delx \right) \cdot \sin\left[\left(\omega_{d1} - delw \right) \cdot t \cdot dt \right] \right]$$

The force and displacement time responses are displayed below.

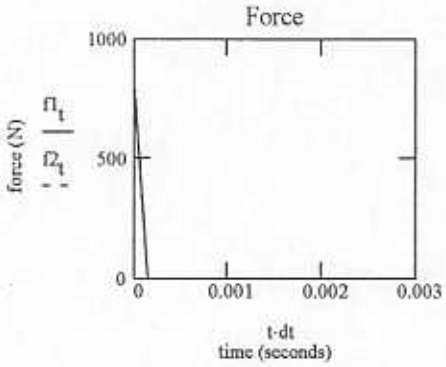

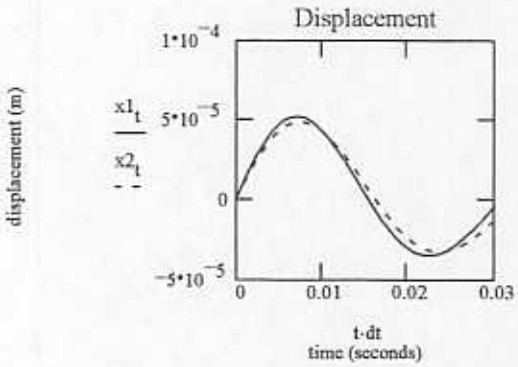

The time domain data is transformed to the frequency domain so that the stiffness and damping coefficients can be identified.

Frequency domain counter

$j := 0, 1 .. 300$

$F1 := \mathrm{fft}(f1)$ $\quad F2 := \mathrm{fft}(f2)$

$X1 := \mathrm{fft}(x1)$ $\quad X2 := \mathrm{fft}(x2)$

Define frequency domain parameters

$f_j := j \cdot \Delta f$ Hz

$w_j := f_j \cdot 2 \cdot \pi$ rad/sec

$w2_j := (w_j)^2$ (rad/sec)^2

The impedances are calculated as follows (seal inertia is not subtracted)

$$H1_j := \frac{F1_j}{X1_j} \quad \text{N/m} \qquad H2_j := \frac{F2_j}{X2_j} \quad \text{N/m}$$

The real and imaginary portions of the impedance are displayed separately below

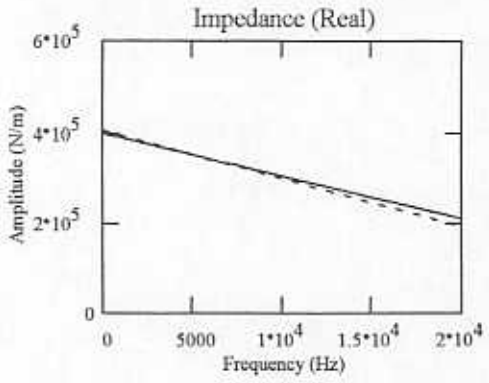

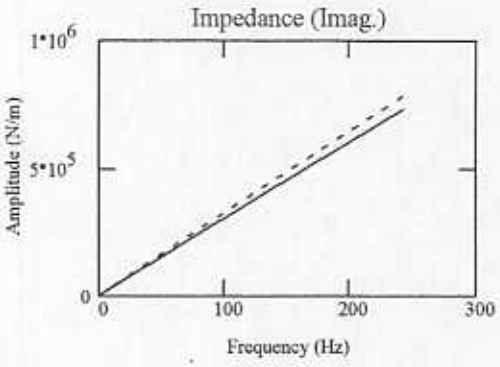

Finally, the stiffness and damping values are identified below, and the uncertainty for each coefficient is the difference between the two identified values

$k1 := \text{intercept}(w2, \text{Re}(H1))$ $\quad$ $c1 := -\text{slope}(w, \text{Im}(H1))$

$k1 = 3.884 \cdot 10^5$ N/m $\quad$ $c1 = 479.655$ N sec/m

$k2 := \text{intercept}(w2, \text{Re}(H2))$ $\quad$ $c2 := -\text{slope}(w, \text{Im}(H2))$

$k2 = 3.94 \cdot 10^5$ N/m $\quad$ $c2 = 513.692$ N sec/m

$$\Delta k := \frac{|k1 - k2|}{2} \qquad \Delta c := \frac{|c1 - c2|}{2}$$

$\Delta k = 2.792 \cdot 10^3$ N/m $\quad$ $\Delta c = 17.019$ N sec/m